Some Statistical Properties of the Burgers Equation with White-Noise Initial Velocity

Patrick Valageas

Abstract We revisit the one-dimensional Burgers equation in the inviscid limit for white-noise initial velocity. We derive the probability distributions of velocity and Lagrangian increments, measured on intervals of any length x. This also gives the velocity structure functions. Next, for the case where the initial density is uniform, we obtain the distribution of the density, over any scale x, and we derive the density two-point correlation and power spectrum. Finally, we consider the Lagrangian displacement field and we derive the distribution of increments of the Lagrangian map. We check that this gives back the well-known mass function of shocks. For all distributions we describe the limiting scaling functions that are obtained in the large-scale and small-scale limits. We also discuss how these results generalize to other initial conditions, or to higher dimensions, and make the connection with a heuristic multifractal formalism. We note that the formation of point-like masses generically leads to a universal small-scale scaling for the density distribution, which is known as the "stable-clustering ansatz" in the cosmological context (where the Burgers dynamics is also known as the "adhesion model").

Keywords Inviscid Burgers equation · Turbulence · Cosmology: large-scale structure of the universe

1 Introduction

The Burgers equation [7], which describes the advection of a velocity field by itself, with a nonzero viscosity, is a very popular nonlinear evolution equation that appears in many physical problems, see [5] for a recent review. It was first introduced as a simplified model of fluid turbulence, as it shares the same hydrodynamical (advective) nonlinearity and several conservation laws with the Navier-Stokes equation. Even though it was shown later on by [19] and [8] that it can be explicitly integrated and lacks the chaotic character associated with actual turbulence, it still retains much interest for hydrodynamical studies, particularly

P. Valageas (✉)
Institut de Physique Théorique, CEA Saclay, 91191 Gif-sur-Yvette, France
e-mail: valag@spht.saclay.cea.fr

as a useful benchmark for approximation schemes [11]. On the other hand, it has appeared in many other physical situations, such as the propagation of nonlinear acoustic waves in nondispersive media [16], the study of disordered systems and pinned manifolds [22], or the formation of large-scale structures in cosmology [17, 35]. There, in the limit of vanishing viscosity, it is known as the "adhesion model" and it provides a good description of the large-scale filamentary structure of the cosmic web [23]. In this context, one is interested in the statistical properties of the dynamics, starting with random Gaussian initial conditions [18, 20] (i.e. "decaying Burgers turbulence" in the hydrodynamical context). Moreover, in addition to the velocity field, one is also interested in the properties of the density field generated by this dynamics, starting with an initial uniform density.

This problem has led to many studies in the inviscid limit, focusing on power-law initial spectra (fractional Brownian motion), $E_0(k) \propto k^n$, especially for the two peculiar cases of white-noise initial velocity ($n = 0$) [7, 12, 20, 28] or Brownian motion initial velocity ($n = -2$) [6, 28, 29, 34]. The initial velocity fluctuations are dominated by short wavelengths in the former case and by large wavelengths in the latter case. Therefore, they provide two simple examples for two more general classes of random initial conditions, associated with $-1 < n < 1$ and $-3 < n < -1$ [16, 18], which show both common and different significant behaviors. For instance, the integral scale of turbulence, $L(t)$, and the tail of the shock mass function, scale with n as $L(t) \sim t^{2/(n+3)}$ and $\ln[n(> m)] \sim -m^{n+3}$ over the whole range $-3 < n < 1$ [18, 24, 25, 28], even though shocks are dense for $-3 < n < -1$ but isolated for $-1 < n < 1$ [28]. Then, the specific advantage of these two cases, $n = 0$ and $n = -2$, is that in both cases the initial velocity field is built from a white-noise stochastic field (either directly or through one integration), which gives rise to Markovian processes and allows to derive many explicit analytical results.

In parallel with a study of the Brownian case in [34], we revisit in this article the white-noise case, taking advantage of the results obtained in [12]. In particular, we pay attention to issues that arise in the hydrodynamical context (velocity structure functions, Lagrangian displacement field) as well as in the cosmological context (statistics of the density field). Thus, the main goal of this article is to provide explicit results for the distributions of velocity increments and density fluctuations. As explained above, this complements the study [34] of the Brownian case, so that we now have explicit exact results for these quantities for the two representative cases $n = 0$ and $n = -2$. This should prove useful to check the validity of approximation schemes devised for generic initial conditions and higher dimensions. as in [33] where the tails of these probability distributions are studied in the general case.

We first describe in Sect. 2 the white-noise initial conditions and the standard geometrical interpretation in terms of parabolas of the Hopf-Cole solution of the dynamics [7]. Then, we recall in Sect. 3 the Eulerian one-point and two-point distributions, $p_x(q)$ and $p_{x_1,x_2}(q_1, q_2)$, associated with the inverse Lagrangian map $x \mapsto q$, that were obtained in [12]. This allows us to derive in Sect. 4 the distributions of the inverse Lagrangian increment and velocity increment, as well as the velocity structure functions. We also describe the limiting large-scale and small-scale distributions. Next, we consider in Sect. 5 the distribution of the density within intervals of size x, and the density two-point correlation and power spectrum. Then, turning to a Lagrangian point of view, we study the Lagrangian displacement field in Sect. 6. Finally, we describe in Sect. 7 how the small-scale scalings shown by these exact results can be generalized to other initial conditions and higher dimensions within a heuristic approach.

2 Initial Conditions and Geometrical Solution

2.1 Equation of Motion

We consider in this article the one-dimensional Burgers equation for the velocity field $v(x, t)$ in the limit of zero viscosity,

$$\frac{\partial v}{\partial t} + v \frac{\partial v}{\partial x} = \nu \frac{\partial^2 v}{\partial x^2} \quad \text{with } \nu \to 0^+. \tag{1}$$

Let us recall here that in the cosmological context, the time t in the Burgers equation (1) actually stands for the linear growing mode $D_+(t)$ of the density fluctuations, the spatial co-ordinate x is a comoving coordinate (that follows the uniform Hubble expansion) and, up to a time-dependent factor, the velocity v is the peculiar velocity (where the Hubble expansion has been subtracted), see [17, 35]. In these coordinates, the evolution of the density field is still given by the continuity equation (37) below, where the density ρ is the comoving density. If we take $\nu = 0$, that is we remove the right-hand side in (1), this is the well-known Zeldovich approximation [32, 37], where particles always keep their initial velocity and merely follow straight trajectories. The diffusive term of (1) is then added as a phenomeno-logical device to prevent particles from escaping to infinity after crossing each other and to mimic the gravitational trapping of particles within the potential wells formed by the over-densities [17]. Of course, this cannot describe the inner structure of collapsed objects (e.g., galaxies) but it provides a good description of the large-scale structure of the cosmic web [23].

As is well known [8, 19], introducing the velocity potential $\psi(x, t)$ and making the change of variable $\psi(x, t) = -2\nu \ln \theta(x, t)$ transforms the nonlinear Burgers equation into the linear heat equation. This gives the explicit solution

$$v(x, t) = \frac{\partial \psi}{\partial x} \quad \text{with } \psi(x, t) = -2\nu \ln \int_{-\infty}^{\infty} \frac{dq}{\sqrt{4\pi \nu t}} \exp\left[-\frac{(x - q)^2}{4\nu t} - \frac{\psi_0(q)}{2\nu}\right], \tag{2}$$

where we introduced the initial condition $\psi_0(q) = \psi(q, t = 0)$. Then, in the limit $\nu \to 0^+$ the steepest-descent method gives

$$\psi(x, t) = \min_q \left[\psi_0(q) + \frac{(x - q)^2}{2t}\right] \quad \text{and} \quad v(x, t) = \frac{x - q(x, t)}{t}, \tag{3}$$

where we introduced the Lagrangian coordinate $q(x, t)$ defined by

$$\psi_0(q) + \frac{(x - q)^2}{2t} \quad \text{is minimum at the point } q = q(x, t). \tag{4}$$

The Eulerian locations x where there are two solutions, $q_- < q_+$, to the minimization prob-lem (4) correspond to shocks (and all the matter initially between q_- and q_+ is gathered at x). The application $q \mapsto x(q, t)$ is usually called the Lagrangian map, and $x \mapsto q(x, t)$ the inverse Lagrangian map (which is discontinuous at shock locations) [5]. For the case of white-noise initial velocity that we consider in this paper, it is known that there is only a finite number of shocks per unit length [3, 28].

2.2 Initial Conditions

In this article, we consider a white-noise initial velocity field $v_0(q)$, normalized by

$$\langle v_0(q) \rangle = 0, \qquad \langle v_0(q_1)v_0(q_2) \rangle = D\,\delta(q_1 - q_2), \tag{5}$$

where $\langle \ldots \rangle$ is the average over all realizations of the initial velocity field. The velocity potential is defined up to a constant, and we may choose to normalize the initial potential $\psi_0(q)$ by $\psi_0(0) = 0$, whence

$$\psi_0(q) = \int_0^q dq'\, v_0(q'), \quad \langle \psi_0(q) \rangle = 0, \quad \langle \psi_0(q_1)\psi_0(q_2) \rangle = D\,q_1, \quad \text{for } 0 \le q_1 \le q_2. \tag{6}$$

Thus, the initial velocity potential is a bilateral Brownian motion that starts from the origin. Then, thanks to the scale invariance of the Brownian motion, the scaled initial potential $\psi_0(\lambda q)$ has the same probability distribution as $\lambda^{1/2}\psi_0(q)$, for any $\lambda > 0$. Hence, using the explicit solution (3) we obtain the scaling laws

$$\psi(x,t) \overset{\text{law}}{=} t^{1/3}\psi(x/t^{2/3}, 1), \qquad v(x,t) \overset{\text{law}}{=} t^{-1/3}v(x/t^{2/3}, 1),$$
$$q(x,t) \overset{\text{law}}{=} t^{2/3}q(x/t^{2/3}, 1), \tag{7}$$

where $\overset{\text{law}}{=}$ means that both sides have the same probability distribution. Thus, any equal-time statistics at a given time $t > 0$ can be expressed in terms of the same quantity at the time $t = 1$ through appropriate rescalings. In this article we only investigate equal-time statistics, so that t can be seen as a mere parameter in the explicit solution (2). Then, it is convenient to introduce the dimensionless coordinates,

$$Q = \frac{q}{\gamma}, \qquad X = \frac{x}{\gamma}, \qquad V = \frac{tv}{\gamma}, \qquad \Psi = \frac{t\psi}{\gamma^2}, \qquad C = \frac{tc}{\gamma^2}, \quad \text{with } \gamma = (2Dt^2)^{1/3}, \tag{8}$$

which express the scaling laws (7) (here c is the parabola height that will be introduced below in (9)). Thus, probability distributions written in terms of these variables no longer depend on time, and the scale $X = 1$ is the characteristic length of the system, at any time. On large quasi-linear scales, $X \gg 1$, density fluctuations are small and the distributions are strongly peaked around their mean, with tails that are directly governed by the initial conditions (but shocks cannot be neglected). On small nonlinear scales, $X \ll 1$, density fluctuations are large (e.g., most Eulerian intervals are empty) and probability distributions show broad power-law regions. These behaviors will be clearly seen in the following sections.

2.3 Geometrical Interpretation

As is well known [7,], the minimization problem (4) has a nice geometrical solution. Indeed, let us consider the downward parabola $\mathcal{P}_{x,c}(q)$ centered at x and of maximum c, i.e. of vertex (x, c), of equation

$$\mathcal{P}_{x,c}(q) = -\frac{(q-x)^2}{2t} + c. \tag{9}$$

Then, starting from below with a large negative value of c, such that the parabola is everywhere well below $\psi_0(q)$ (this is possible thanks to the scaling $\psi_0(\lambda q) \overset{\text{law}}{=} \lambda^{1/2}\psi_0(q)$ which

shows that $\psi_0(q)$ only grows as $|q|^{1/2}$ at large $|q|$), we increase c until the two curves touch one another. Then, the abscissa of the point of contact is the Lagrangian coordinate $q(x, t)$ and the potential is given by $\psi(x, t) = c$. In order to use this geometrical construction, it will be more convenient in the following to normalize the potential ψ_0 by $\psi_0(q_-) = 0$, where we first restrict the system to the finite interval $[q_-, q_+]$, and to eventually take the limits $q_\pm \to \pm\infty$ [12], instead of normalizing at the origin $q = 0$ as in (6). Indeed, this avoids making the point $q = 0$ artificially play a special role. With this choice, the initial potential $\psi_0(q)$ is a single Brownian motion that starts from the left boundary q_-.

For the white-noise initial conditions (5), the process $q \mapsto \psi_0$ is Markovian. Then, following the approach of [12], from the geometrical construction (9) one can see that a key quantity is the conditional probability density $K_{x,c}(q_1, \psi_1; q_2, \psi_2)$ for the Markov process $\psi_0(q)$, starting from ψ_1 at q_1, to end at ψ_2 at $q_2 \geq q_1$, while staying above the parabolic barrier, $\psi_0(q) > \mathcal{P}_{x,c}(q)$, for $q_1 \leq q \leq q_2$. This kernel was obtained in [12] and we recall its expression in Appendix A with our notations. We also derive the closely related kernel $E_{x,c}(q_1, \psi_1; q_2, \psi_2; q)$, defined in (99), which only counts among these initial conditions the ones that have a last excursion below $\mathcal{P}_{x,c+dc}$ in the range $[q, q + dq]$.

3 Known Eulerian Distributions

We briefly recall in this section the expressions of the one-point distributions, $p_x(q)$ and $p_x(v)$, of the Lagrangian coordinate $q(x, t)$ and velocity $v(x, t)$ at the Eulerian point x. We also consider the two-point distributions $p_{x_1,x_2}(q_1, q_2)$ and $p_{x_1,x_2}(q_1, q_2)$. These results were already obtained in [12], but they are the basis of our computation in the following sections of the distributions of Lagrangian and velocity increments, from which we obtain the distribution of the matter density, and of the distribution of the Eulerian increment. We give more details and explicit expressions in Appendix B.

3.1 One-Point Eulerian Distributions $p_x(q)$ and $p_x(v)$

To any Eulerian point x we can associate the Lagrangian coordinate $q(x, t)$ defined as the location of the minimum in (4), except at shock locations where there are two (or more) contact points between the initial potential $\psi_0(q)$ and the first-contact parabola $\mathcal{P}_{x,c}$. Since shocks are in finite number per unit length [3, 28], Eulerian points have a well-defined Lagrangian coordinate $q(x, t)$ with probability one. However, note that the Eulerian position x is usually not "occupied" by the infinitesimal mass that was initially located at q, as all the matter is collected within shocks (thus a given Eulerian point has almost surely a zero matter density) [35]. Nevertheless, through (3) one can derive the properties of the velocity field from the Lagrangian coordinate $q(x, t)$.

The one-point distribution, $p_x(q)$, of the Lagrangian coordinate q at point x, can be readily obtained from the kernel $E_{x,c}$ given in (101), or the kernel $K_{x,c}$, as shown in [12]. For instance, from the definition of $E_{x,c}$ we can write

$$p_x(q) = \lim_{q_\pm \to \pm\infty} \int dc \, d\psi_+ \, E_{x,c}(q_-, 0; q_+, \psi_+; q), \tag{10}$$

where we normalized the initial potential by $\psi_0(q_-) = 0$ and we let $q_\pm \to \pm\infty$ as the size of the system goes to infinity, as discussed below (9). Thus, in (10) we count all initial conditions $\psi_0(q)$ that have a first-contact point of abscissa q with a parabola $\mathcal{P}_{x,c}$, and we integrate over all possible heights c. We recall in Appendix B.1 the explicit expressions of

$P_X(Q)$ and $P_X(V)$, in terms of the scaling variables (8), see (102)–(103) and [12]. Both distributions are related through the change of variable $X = Q + V$, that expresses the second equation (3). Thanks to the homogeneity and isotropy of the system, the distribution $P_X(Q)$ only depends on the distance $|Q - X|$, whereas $P(V)$ is even and no longer depends on X. The asymptotic behavior of the distribution of the velocity V (and of the Lagrangian coordinate $Q = X - V$),

$$|V| \gg 1: \quad P(V) \sim \frac{2|V|}{\mathrm{Ai}'(-\omega_1)} e^{-\omega_1|V| - |V|^3/3}, \qquad (11)$$

shows that $P(V)$ decreases faster than a Gaussian at large V [2, 12]. Contrary to cases where the initial velocity field has no ultraviolet divergence (i.e. the initial variance $\sigma_{v_0}^2(0) = \langle v_0^2 \rangle$ is finite, as for the case of Brownian initial velocity [34]), the large-v tail cannot be directly understood from the statistics of rare local peaks in the initial velocity field, Here, as we have recalled above, at any time $t > 0$ all the matter has collapsed within a finite number of shocks per unit length, which merge in the course of time to build increasingly massive shocks within larger voids [3, 12, 28]. Then, the typical velocities observed in the system are governed by this merging process, rather than by the initial velocities of regular points that would not have collided yet. Nevertheless, the cubic exponential tail (11) can be understood as follows. A structure with a large velocity v has traveled by time t over a distance of order $x \sim vt$. On the other hand, the mean velocity $\bar{v}_0(q)$ of the mass that was initially located in the Lagrangian interval $[q_1, q_2]$, of size $q = q_2 - q_1$, is $\bar{v}_0(q) = \int_{q_1}^{q_2} dq'\, v_0(q')/q = (\psi_2 - \psi_1)/q$. It is Gaussian with a variance $\sigma_{\bar{v}_0}^2(q) = D/q$ from (6). Since momentum is conserved by the inviscid Burgers dynamics [7], so that the momentum of a shock is equal to the sum of the initial momenta of all the particles it contains, we can associate to the velocity v and the distance $x = vt$ the Gaussian weight $\sim e^{-v^2/\sigma_{\bar{v}_0}^2(vt)} \sim e^{-v^3 t/D}$, where we did not write numerical factors in the exponential. This gives back the cubic exponential tail (11). Even though we followed shocks in the previous argument, in spite of the fact that they occupy a set of zero measure in Eulerian space, this still sets the tail of the Eulerian velocity field as the velocity of a shock located at position x is related to the local velocity field as $v^{\mathrm{shock}} = (v(x^-) + v(x^+))/2$, and $v(x, t)$ has a constant slope of $1/t$ in-between shocks, see [7]. Cubic exponential tails such as (11) are characteristic of probability distributions obtained for these white-noise initial conditions [2, 3, 12].

3.2 Two-Point Eulerian Distributions $p_{x_1,x_2}(q_1, q_2)$ and $p_{x_1,x_2}(v_1, v_2)$

We now consider the two-point distribution, $p_{x_1,x_2}(q_1, q_2)$, of the Lagrangian coordinates $\{q_1, q_2\}$ associated with the Eulerian locations $\{x_1, x_2\}$. We take $x_1 < x_2$, which implies that $q_1 \leq q_2$ since particles do not cross each other and therefore remain well-ordered. One needs to consider the two cases, i) $q_1 \neq q_2$, and ii) $q_1 = q_2$. The first case, associated with different first-contact points, gives the contribution [12]

$$P_{X_1,X_2}^{\neq}(Q_1, Q_2) = \theta(Q_2 - Q_1)\, \mathcal{J}(Q_1 - X_1)\, \mathcal{J}(X_2 - Q_2)\, \mathcal{H}_{X_1,X_2}(Q_1, Q_2), \qquad (12)$$

where $\theta(Q_2 - Q_1)$ is the Heaviside function and we introduced the functions $\mathcal{J}$ and $\mathcal{H}$ given by (103) and (106), whereas the second case, associated with a common first-contact point, gives the contribution

$$P_{X_1,X_2}^{=}(Q_1, Q_2) = \delta(Q_2 - Q_1)\, \mathcal{J}(Q_1 - X_1)\, \mathcal{J}(X_2 - Q_2)\, e^{-(Q_1 - X_1)^3/3 + (Q_2 - X_2)^3/3}. \qquad (13)$$

One can check that the function $\mathcal{H}_{X_1,X_2}(Q_1, Q_2)$, whence the contribution $P^{\neq}_{X_1,X_2}(Q_1, Q_2)$, and the contribution $P^{=}_{X_1,X_2}(Q_1, Q_2)$ are invariant with respect to uniform translations of X_i and Q_i, in agreement with the statistical homogeneity of the system. Then, the full distribution $P_{X_1,X_2}(Q_1, Q_2)$ is given by the sum of both contributions (12) and (13). Next, the two-point velocity distribution, $P_{X_1,X_2}(V_1, V_2)$, is obtained from (12), (13), by using $V_i = X_i - Q_i$.

We can note here that, thanks to the Markovian character of the process $q \mapsto \psi_0(q)$, the n-point distributions of the velocities v_i, and of the Lagrangian coordinates q_i, factorize as [12]

$$p_{x_1,\ldots,x_n}(v_1, \ldots, v_n) = p_{x_1}(v_1)\, p(x_2, v_2|x_1, v_1) \cdots p(x_n, v_n|x_{n-1}, v_{n-1}), \tag{14}$$

and

$$p_{x_1,\ldots,x_n}(q_1, \ldots, q_n) = p_{x_1}(q_1)\, p(x_2, q_2|x_1, q_1) \cdots p(x_n, q_n|x_{n-1}, q_{n-1}), \tag{15}$$

with the transition kernels

$$p(x_2, v_2|x_1, v_1) = \frac{p_{x_1,x_2}(v_1, v_2)}{p_{x_1}(v_1)} \quad \text{and} \quad p(x_2, q_2|x_1, q_1) = \frac{p_{x_1,x_2}(q_1, q_2)}{p_{x_1}(q_1)}, \tag{16}$$

that can be obtained from the two-point and one-point distributions derived above. Again, the kernels $p(x_2, v_2|x_1, v_1)$ and $p(x_2, q_2|x_1, q_1)$ are invariant with respect to uniform translations of the spatial coordinates x_i and q_i. However, contrary to the case of Brownian initial velocity [6, 34], the transition kernel does not only depend on the two relative distances $x_2 - x_1$ and $q_2 - q_1$ (thus it also depends on the third distance $q_1 - x_1$). This means that the inverse Lagrangian map, $x \mapsto q$, does not have independent increments.

4 Probability Distributions of the Lagrangian and Velocity Increments

We now consider the probability distributions, $p_x(q)$ and $p_x(v)$, of the Lagrangian increment, $q = q_2 - q_1$, and of the velocity increment, $v = v_2 - v_1$, over the Eulerian distance $x = x_2 - x_1$. These distributions can be directly obtained from the two-point distributions (12) and (13), but they were not studied in previous works (except for the singular part (108) associated with voids). In particular, as noticed in the conclusion of [12], the asymptotics of $p_x(v)$ at large v cannot be obtained in a straightforward manner from the estimations of their Sect. 5, as the latter apply to the limit of large distance x at fixed v_1 and v_2. Next, we shall need the distribution $p_x(q)$ to derive the distribution of the overdensity at scale x in Sect. 5.

4.1 Lagrangian Increment, $q = q_2 - q_1$, and Velocity Increment, $v = v_2 - v_1$

The probability distribution $P_X(Q)$ of the Lagrangian increment, $Q = Q_2 - Q_1$, can be obtained by integrating the sum of the bivariate distributions (12) and (13) over the variable Q_1 at fixed $Q = Q_2 - Q_1$. This gives

$$P_X(Q) = \int_{-\infty}^{\infty} \mathrm{d}Q_1\, \mathcal{J}(Q_1)\, \mathcal{J}(X - Q - Q_1)\big[\theta(Q)\mathcal{H}_{0,X}(Q_1, Q_1 + Q)$$
$$+ \delta(Q)e^{-Q_1^3/3 + (Q_1 - X)^3/3}\big], \tag{17}$$

where $\theta(Q)$ is the Heaviside function. The second term gives a contribution of the form $P_X^=(Q) = \delta(Q) P_X^0$, given by (108) in Appendix B.3. Note that Eulerian intervals with $Q = 0$ also have a zero matter content so that P_X^0 is also the probability for an interval of size X to be empty (see Sect. 5 below where we discuss the matter density field), in agreement with the result obtained in [12] for this void probability. We recall the properties of this distribution of voids in Appendix B.3 and Fig. 12.

In this article we are mostly interested in the regular part, $P_X^{\neq}(Q)$, associated with non-empty Eulerian intervals, which has not been studied in previous works. From the first term in expression (17) it reads as

$$P_X^{\neq}(Q) = \theta(Q) 2\sqrt{\pi X} e^{-X^3/12} \int_{-i\infty}^{+i\infty} \frac{ds\, ds_1\, ds_2}{(2\pi i)^3} \frac{e^{s(Q-X)+(s_1+s_2)X/2+(s_1-s_2)^2/(4X)}}{\mathrm{Ai}(s_1)\mathrm{Ai}(s_2)\mathrm{Ai}(s_1-s)\mathrm{Ai}(s_2-s)}$$

$$\times \int_0^\infty dr\, e^{Xr} \mathrm{Ai}(r+s_1)\mathrm{Ai}(r+s_2). \tag{18}$$

We recall in Appendix C an alternative expression for the integral over r that appears in (18), obtained in [12], which is useful to derive asymptotic behaviors. Thus, at large distances, $X \gg 1$, (18) yields the asymptotic behaviors

$$X \gg 1: \quad P_X^{\neq}(Q) \sim \frac{\sqrt{X}}{\mathrm{Ai}'(-\omega_1)^2} Q^{-1/2} e^{-\omega_1 X - X^3/12} \quad \text{for } 0 < Q \ll X^{-2}, \tag{19}$$

$$P_X^{\neq}(Q) \sim \frac{\sqrt{\pi}}{\mathrm{Ai}'(-\omega_1)^2} |V|^{3/2} e^{-\omega_1 |V| - |V|^3/12} \quad \text{for } |V| \gg 1 \text{ and } Q \gg X^{-2}, \tag{20}$$

where $V = X - Q$ is the dimensionless velocity as in (8). At small distances, $X \ll 1$, (18) leads to

$$X \ll 1: \quad P_X^{\neq}(Q) \sim \frac{X}{\sqrt{\pi}} Q^{-1/2} \quad\quad\quad \text{for } 0 < Q \ll 1, \tag{21}$$

$$P_X^{\neq}(Q) \sim 2\sqrt{\pi} X Q^{5/2} e^{-\omega_1 Q - Q^3/12} \quad \text{for } 1 \ll Q \ll X^{-1/2}, \tag{22}$$

$$P_X^{\neq}(Q) \sim 2\pi \sqrt{X} Q^{3/2} e^{-\omega_1 Q - Q^3/12} \quad \text{for } Q \gg X^{-1/2}. \tag{23}$$

Thus, at all scales X the distribution $P_X^{\neq}(Q)$ displays an inverse square root tail at low Q. At large X this tail has an exponentially small weight, that scales as the weight P_X^0 of the empty cells, and it is restricted to very low Q, whereas at small X it describes the full low-Q regime. As expected, we can check from (20) that on large scales, $X \gg 1$, the Lagrangian increment is centered on X, with the usual cubic exponential tails encountered for this white-noise initial velocity spectrum, whereas on small scales, $X \ll 1$, the distribution shows a monotonous decline.

We display in Fig. 1 the probability distribution $P_X(Q)$ for three Eulerian sizes. This clearly shows the change of shape as we go from large to small scales, as well as the translation of the mean $\langle Q \rangle$, that follows X from the conservation of matter (see (38) below). Note that for numerical purposes, in order to follow the evolution of $P_X(Q)$ with X, and its behavior over the different characteristic domains listed in (19)–(23), it is useful to gradually move the integration contours in the complex plane of (18) as one goes from one regime to another one (but making sure that one does not cross singularities). One interest of these results is to provide an explicit example that is representative of initial conditions in the
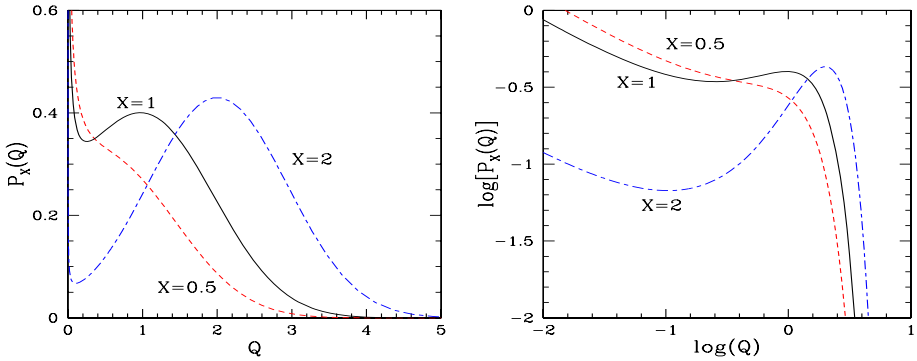
Fig. 1 (Color online) *Left panel:* The probability distribution $P_X(Q)$ of the Lagrangian increment Q, for three Eulerian sizes, $X = 0.5, 1$ and 2, from (18). We have $Q \geq 0$ and all curves display an inverse square root singularity $\propto 1/\sqrt{Q}$ at $Q \to 0^+$. In addition, there is a Dirac contribution, $P_X^0 \delta(Q)$, with the weight P_X^0 displayed in Fig. 12. *Right panel:* Same as *left panel* but on a logarithmic scale
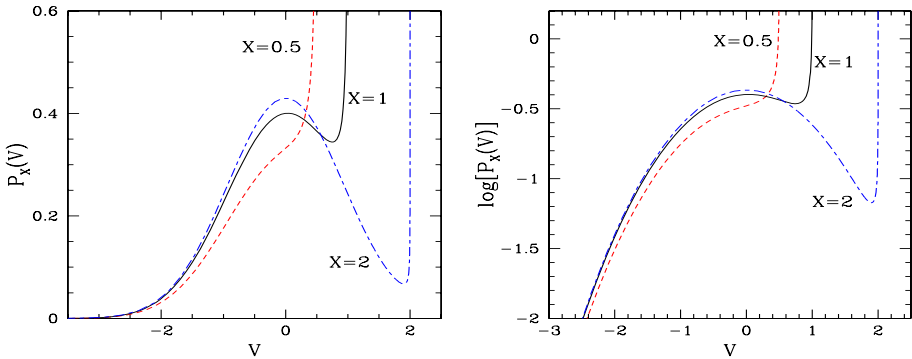

Fig. 2 (Color online) *Left panel:* The probability distribution $P_X(V)$ of the velocity increment V, for three Eulerian sizes, $X = 0.5, 1$ and 2, from (18). We have $V \leq X$ and all curves display an inverse square root singularity $\propto 1/\sqrt{X-V}$ at $V \to X^-$. In addition, there is a Dirac contribution, $P_X^0 \delta(X - V)$, with the weight P_X^0 displayed in Fig. 12. *Right panel:* Same as *left panel* but on a semi-logarithmic scale

range $-1 < n < 1$, where n is the slope of the initial energy spectrum (i.e. $E_0(k) \propto k^{n+1-D}$ in D dimensions), which show significant power at high wavenumbers. Then, we can see that the distribution $P_X^{\neq}(Q)$ always diverges at low Q (i.e. at low density) as $1/\sqrt{Q}$. This implies in particular that, contrary to the cases $-3 < n < -1$, the very low-Q part of the distribution cannot be estimated through steepest-descent approaches that apply to rare events, as discussed in [33]. Nevertheless, these approaches can give an estimate of $P_X^{\neq}(Q)$ in the quasi-linear limit $X \to \infty$ at fixed Q, studied in Sect. 4.2 below.

The probability distribution, $P_X(V)$, of the velocity increment, $V = V_2 - V_1$, is obtained from the distribution $P_X(Q)$ by using the relation $V = X - Q$. We show our results in Fig. 2, for the same three Eulerian scales as for $P_X(Q)$ displayed in Fig. 1. There is no longer a translation of the typical velocity, since $\langle V \rangle = 0$ for any scale X, but we clearly see the translation of the inverse-square root tail, $\sim 1/\sqrt{X-V}$, that follows the upper bound

$V \leq X$ associated with empty cells (as seen from the relation $X = Q + V$ and the constraint $Q \geq 0$).

4.2 Asymptotic Distribution on Large Scales

On large scales, $X \gg 1$, the distributions $P_X(Q)$ and $P_X(V)$, except for the exponentially small contributions associated with $Q = 0$ and $Q \ll X^{-2}$ in (108) and (19), can be described by the symmetric distribution $\mathcal{F}_\infty$,

$$X \gg 1: \quad P_X(Q) \sim \mathcal{F}_\infty(X - Q) \quad \text{and} \quad P_X(V) \sim \mathcal{F}_\infty(V), \tag{24}$$

with a Fourier transform $\hat{\mathcal{F}}_\infty$ given by:

$$\mathcal{F}_\infty(V) = \int_{-\infty}^{\infty} \frac{dk}{2\pi} e^{ikV} \hat{\mathcal{F}}_\infty(k) \quad \text{with} \quad \hat{\mathcal{F}}_\infty(k) = \left(\int_{-i\infty}^{+i\infty} \frac{ds'}{2\pi i} \frac{1}{\mathrm{Ai}(s')\mathrm{Ai}(s' + ik)} \right)^2. \tag{25}$$

Equation (25) is obtained from (18) by using the asymptotic behavior of the integral over r, as given by the first term in (111), and next making the change of variable $s = ik$. The scaling function $\mathcal{F}_\infty(V)$ no longer depends on X: the distribution of the velocity increment V converges to the finite distribution $\mathcal{F}_\infty$ on large scales $X \to \infty$. Note that in this limit the upper boundary on V, $V \leq X$, associated with the positivity of $Q = X - V$, goes to $+\infty$ so that the limiting function $\mathcal{F}_\infty(V)$ is defined over the whole real axis. This is also why the Laplace transform (18) naturally gives rise to the Fourier transform (25) in this limit. Moreover, we can see from (25) that $\mathcal{F}_\infty(V)$ is even (the change of integration variable $s' \to s' - ik/2$ in (25) readily shows that $\hat{\mathcal{F}}_\infty(k)$ is even). The asymptotic behaviors of $\mathcal{F}_\infty(V)$ at large V can be read from (20):

$$|V| \gg 1: \quad \mathcal{F}_\infty(V) \sim \frac{\sqrt{\pi}}{\mathrm{Ai}'(-\omega_1)^2} |V|^{3/2} e^{-\omega_1 |V| - |V|^3/12}. \tag{26}$$

Thus, we recover the cubic exponential tails that are characteristic of white-noise initial conditions [2, 3, 12] and can be understood at a qualitative level following the discussion below (11). In fact, as shown in [33], on a quantitative level it is possible to obtain the factor $1/12$ in the exponential (26) through a simple steepest-descent approach, that identifies the initial conditions (i.e. the relevant saddle-points) that give the main contribution to these tails. Then, the exact result (26) provides a useful nontrivial test of such general approaches that rest on some additional assumptions (for instance, one only looks for symmetric saddle-points).

Of course, the scaling function $\mathcal{F}_\infty(V)$ does not capture the low-Q power-law tail (19). However, using the property

$$\int_{-i\infty}^{+i\infty} \frac{ds}{2\pi i} \frac{1}{\mathrm{Ai}(s)^2} = 1, \tag{27}$$

we can see that the distribution $\mathcal{F}_\infty(V)$ is normalized to unity as it should, since the weights of the low-Q tail (19) and of the Dirac term (108) vanish in the limit $X \to \infty$. We show the scaling function $\mathcal{F}_\infty(V)$ in Fig. 3.

From (24)–(25), the moments of the velocity increment are given in this limit by

$$X \to +\infty: \quad \langle V^{2n+1} \rangle = 0, \quad \langle V^{2n} \rangle = (-1)^n \frac{d^{2n}\hat{\mathcal{F}}_\infty}{dk^{2n}}(0), \tag{28}$$
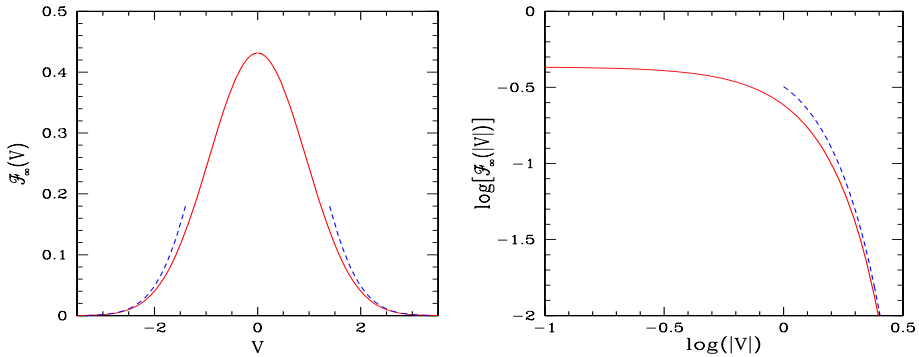
Fig. 3 (Color online) *Left panel:* The asymptotic distribution $\mathcal{F}_\infty(V)$ of the velocity increment V, reached in the limit of large Eulerian distance $X \gg 1$, from (25). The *dashed lines* show the asymptotic behavior (26). *Right panel:* Same as *left panel* but on a logarithmic scale

whence

$$\langle V \rangle = 0 \quad \text{and} \quad \langle Q \rangle = X, \quad \langle V^2 \rangle = \langle Q^2 \rangle_c = -\frac{2}{3} \int_{-i\infty}^{+i\infty} \frac{ds}{2\pi i} \frac{s}{\mathrm{Ai}(s)^2} \simeq 0.837. \quad (29)$$

We can check that we recover $\langle Q \rangle = X$, as implied by the conservation of matter. We can see that there is negligible power on large scales since $\langle Q^2 \rangle_c$ goes to a constant for $X \to +\infty$. This holds for cumulants of all orders, as the scaling function $\mathcal{F}_\infty(V)$ does not depend on X (see also the left panel of Fig. 6, where we can see that both $\langle Q^2 \rangle_c$ and $\langle Q^4 \rangle_c$ have a finite nonzero large-scale limit whereas $\langle Q^3 \rangle_c$ vanishes by symmetry of $\mathcal{F}_\infty$).

Equations (24)–(26) and (28) show that, because of the lack of power at large scales in the initial velocity field, at any time $t > 0$ the system observed at any scale x, whatever large, is governed by nonlinear effects and exhibits strongly non-Gaussian statistics, even though the initial conditions are Gaussian. Indeed, the redistribution of matter within a series of discrete shocks has regularized the initially singular white-noise velocity field, through the balance between the infinite different sign velocities of neighboring particles, over lengths of order $(2Dt^2)^{1/3}$, that have merged in a single shock. Moreover, the velocity field in the voids is governed by the motion of the boundary shocks, since from (3) it has a constant slope $1/t$ in-between shocks, and the velocity of a shock satisfies $v^{\mathrm{shock}} = (v(x^-) + v(x^+))/2$, see [7]. These processes are clearly nonperturbative and give rise to the non-Gaussian statistical properties described above in the large-scale limit. This would not be the case for initial conditions with significant initial power on large scales. Then, even though shocks may have formed as soon as $t > 0$, one still recovers the initial Gaussian statistics on large scales, as explicitly checked in [34] for the case of a Brownian initial velocity field (where the initial energy spectrum is $E_0(k) \propto k^{-2}$ instead of the constant spectrum associated with the white-noise initial condition studied in the present article).

Again, these exact results provide a useful confirmation of the results obtained by approximate methods, such as the steepest-descent approach of [33]. Indeed, there it is found that for $n > D - 3$, which includes the case $\{n = 0, D = 1\}$ studied in this article, the relevant saddle-points always give rise to shocks, which is not the case for initial conditions with less initial power at high wavenumbers (such as $\{n = -2, D = 1\}$, i.e. Brownian 1-D initial velocity).

4.3 Asymptotic Distribution on Small Scales

On small scales, apart from the Dirac contribution (108), associated with empty cells, and the very large-Q tail (23), the distributions $P_X(Q)$ and $P_X(V)$ can be described by the function $\mathcal{F}_0$,

$$X \ll 1: \quad P_X(Q) \sim X \, \mathcal{F}_0(Q) \quad \text{with } Q > 0 \quad \text{and} \quad \mathcal{F}_0(Q) = \int_{-i\infty}^{+i\infty} \frac{\mathrm{d}s}{2\pi \mathrm{i}} \, e^{sQ} \, \tilde{\mathcal{F}}_0(s), \quad (30)$$

with

$$\tilde{\mathcal{F}}_0(s) = -2 \int_{-i\infty}^{+i\infty} \frac{\mathrm{d}s'}{2\pi \mathrm{i}} \frac{1}{\mathrm{Ai}(s')^2} \frac{\partial}{\partial s'} \frac{\mathrm{Ai}'(s'+s)}{\mathrm{Ai}(s'+s)} = -4 \int_{-i\infty}^{+i\infty} \frac{\mathrm{d}s'}{2\pi \mathrm{i}} \frac{\mathrm{Ai}'(s')\mathrm{Ai}'(s'+s)}{\mathrm{Ai}(s')^3 \mathrm{Ai}(s'+s)}. \quad (31)$$

The expressions (30)–(31) are obtained from (18) by taking the Gaussian integration over s_2 (since $|s_2 - s_1| \sim \sqrt{X}$ we can set at leading order $s_2 = s_1$ in (18), apart from the Gaussian factor $e^{(s_1-s_2)^2/(4X)}$), and next setting $X = 0$, which allows to perform the integral over r. Note that a change of variable and an integration by parts allow to write $\mathcal{F}_0(Q)$ as

$$\mathcal{F}_0(Q) = 2Q \left(\int_{-i\infty}^{+i\infty} \frac{\mathrm{d}s'}{2\pi \mathrm{i}} \frac{e^{-s'Q}}{\mathrm{Ai}(s')^2} \right) \left(\int_{-i\infty}^{+i\infty} \frac{\mathrm{d}s}{2\pi \mathrm{i}} \, e^{sQ} \frac{\mathrm{Ai}'(s)}{\mathrm{Ai}(s)} \right). \quad (32)$$

It is clear that the integral over Q of the distribution (30) is not normalized to unity since it decreases as X at small Eulerian distance. Indeed, in this limit almost all Eulerian cells have a zero Lagrangian increment (whence a zero matter density), associated with the Dirac contribution (108) (see the first limit in (109)), whereas nonempty cells occur with a probability proportional to X, see (21)–(23). This can be directly understood from the fact that all the matter is condensed into discrete shocks that occur in a finite number per unit length [3, 28], so that the probability for an Eulerian interval to contain at least one shock (which is equal to $1 - P_X^0$) scales as X for small cell size X.

In fact, the comparison of (32) with results obtained in [12] shows that $\mathcal{F}_0(Q)$ is also the mass function of shocks, as we shall check in Sect. 6.3 below through a different method. Therefore, the expression (30) actually means that on small scales the probability distribution $P_X(Q)$ is asymptotically equal to the probability to encounter one shock of strength Q in the interval of size X. Indeed, since shocks are isolated it is clear that in the limit of small size X the probability to have two or more shocks within X goes to zero faster than X, so that $P_X(Q)$ is governed by the probability to encounter one shock over the length X, which directly gives the scaling (30) where $\mathcal{F}_0(Q)$ would be defined as the shock mass function. Thus, how results explicitly show how the scaling (30) and the shock mass function $\mathcal{F}_0(Q)$ arise from the full distribution (18) of the Lagrangian increment Q.

This property is well-known to hold for any Burgers system without dense shocks [14, 30]. Then, as pointed out in [30], who studied the case of compactly supported white-noise initial velocity, the statistics of the velocity field (whence of the Lagrangian increment Q) at scales much smaller than the average distance between shocks are fully determined by the one-point distribution of shock strength $n(m)$ (which in our case is equal to $\mathcal{F}_0(Q)$ as seen in (77) below). As noticed in [30], the case of compact initial conditions is in a different universality class than the system studied here, where the white-noise initial velocity (5) extends to the whole real line, in the sense that the scalings (8) no longer hold. Indeed, the size L of the initially nonzero velocity field introduces a new scale and at late times there are only two shocks left, which allows [30] to compute both single- and multiple time-velocity
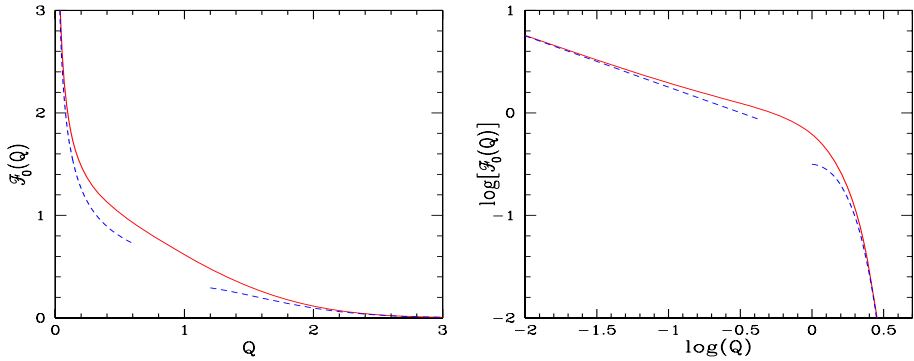
Fig. 4 (Color online) *Left panel:* The scaling function $\mathcal{F}_0(Q)$ that describes the distribution of the Lagrangian increment Q in the limit $X \ll 1$, from (30)–(31). This is also the mass function of shocks, as checked in (77) below. The *dashed lines* are the asymptotic behaviors (33). *Right panel:* Same as *left panel* but on a logarithmic scale

structure functions. Nevertheless, on small scales, much below the typical distance between shocks, both systems show the same scalings (see (35) and (36) below), governed by the one-shock contribution.

Again the asymptotic behaviors can be read from (21)–(23):

$$Q \ll 1: \quad \mathcal{F}_0(Q) \sim \frac{1}{\sqrt{\pi Q}}, \qquad Q \gg 1: \quad \mathcal{F}_0(Q) \sim 2\sqrt{\pi}\, Q^{5/2}\, e^{-\omega_1 Q - Q^3/12}. \tag{33}$$

We show the function $\mathcal{F}_0(Q)$ and its asymptotic tails (33) in Fig. 4, see also [12]. Note that the scaling function $\mathcal{F}_0(Q)$ does not describe the very far tail $Q \gg X^{-1/2}$ of (23), which is repelled to infinity in the limit $X \to 0$. This very high-Q tail is related to the behavior of $P_X(Q)$ at large scales, as seen from the comparison with (23). Indeed, it corresponds to the limit of very rare events, where the tail of the distribution is governed by specific initial conditions, independently of the scale X. These are the saddle-points obtained in [33], which set the cubic exponential falloffs of both (20) and (23). Thus, for any finite X the very far tail (23) of the distributions $P_X(Q)$ and $P_X(V)$ is not captured by the shock mass function, but this regime is repelled to infinity as $X \to 0$.

For any $\nu > 0$, where the contribution from the Dirac term (108) vanishes, we obtain for the moments of the Lagrangian increment

$$\nu > 0: \quad \langle Q^\nu \rangle \sim X\, \Gamma[\nu + 1] \int_{-i\infty}^{+i\infty} \frac{ds}{2\pi i}\, (-s)^{-\nu-1}\, \tilde{\mathcal{F}}_0(s), \tag{34}$$

where the integration contour runs to the left of the origin, $\Re(s) < 0$. Thus, we recover the fractality of the inverse Lagrangian map, $\langle Q^\nu \rangle \propto X$, which is well known to be due to the contribution from shocks as discussed above [14, 30]. Indeed, if we have a shock of finite Lagrangian length δQ_s at position X_s, it gives a contribution $[Q(X_s + X/2) - Q(X_s - X/2)]^\nu \sim (\delta Q_s)^\nu$ which remains of order unity for $X \to 0^+$ for any $\nu > 0$. Next, the probability to have a shock of a given finite strength δQ_s in a small Eulerian interval X scales as X at small distances, which gives rise to the factor X in (34). Therefore, the scaling (34) is actually quite general and applies as soon as shocks have formed with a finite probability [14, 30], above a critical exponent ν_c that depends on the initial conditions (here

$v_c = 0$). We can note that the moments diverge for $v < 0$ because of the Dirac contribution (108), whereas for other initial conditions such as a Brownian initial velocity they can remain well-defined and obey a second scaling law below v_c [1, 34]. For integer v we obtain:

$$n \geq 1: \quad \langle Q^n \rangle \sim X \, (-1)^n \, \frac{\mathrm{d}^n \tilde{\mathcal{F}}_0}{\mathrm{d}s^n}(0), \quad \text{whence } \langle Q \rangle \sim X,$$

$$\langle Q^2 \rangle \sim X \frac{16}{15} \int_{-i\infty}^{+i\infty} \frac{\mathrm{d}s}{2\pi \mathrm{i}} \frac{s^2}{\mathrm{Ai}(s)^2} \simeq 1.136 \, X. \tag{35}$$

Again, we can check that $\langle Q \rangle = X$, in agreement with the conservation of matter. The scaling (35) also implies for the cumulants $\langle Q^n \rangle_c \propto X$ in the small-scale limit $X \ll 1$, as can be checked in the left panel of Fig. 6. This gives for the moments of the velocity increment

$$\langle V \rangle = 0 \quad \text{and for } n \geq 2: \quad \langle V^n \rangle \sim X \frac{\mathrm{d}^n \tilde{\mathcal{F}}_0}{\mathrm{d}s^n}(0),$$

$$\langle [v(x_2, t) - v(x_1, t)]^n \rangle \sim \tilde{\mathcal{F}}_0^{(n)}(0) \left(\frac{2D}{t} \right)^{n/3} \frac{x_2 - x_1}{(2Dt^2)^{1/3}}. \tag{36}$$

Thus, we recover the usual anomalous scaling of the structure functions, $\langle [v(x + \ell) - v(x)]^n \rangle \propto \ell$ at small distance ℓ, that was also observed in numerical simulations [28]. As explained above, this is due to the contribution from shocks [14, 30]. We further discuss these small-scale scalings in Sect. 7.1 below, on a more general setting.

5 Density Field

5.1 Distribution of the Overdensity η as a Function of Scale x

We now consider the evolution of the density field, $\rho(x, t)$, that is generated by the Burgers velocity field, starting at $t = 0$ with a uniform density ρ_0. Thus, the density field obeys the usual continuity equation,

$$\frac{\partial \rho}{\partial t} + \frac{\partial}{\partial x}(\rho v) = 0 \quad \text{with } \rho(x, 0) = \rho_0, \tag{37}$$

whereas the velocity field evolves through the Burgers equation (1). As recalled in the introduction, in the cosmological context this also provides an approximation for the formation of large-scale structures (the cosmic web), known as the "adhesion model" [17, 35]. Then, the density ρ is the comoving density (i.e. measured in comoving coordinates x that follow the Hubble expansion) and t is linear growing mode D_+. Thanks to the conservation of matter, the mass m located between the Eulerian positions $x_1 < x_2$ is $m = \rho_0(q_2 - q_1)$, where $q(x, t)$ is the inverse Lagrangian map. Then, the overall overdensity, $\eta = m/(\rho_0 x)$, in the interval of size $x = x_2 - x_1$, is given by $\eta = q/x = Q/X$. Thus, the probability distribution, $P_X(\eta)$, of the overdensity η, is given by the distribution, $P_X(Q)$, of the Lagrangian increment Q, through

$$\eta = \frac{m}{\rho_0 x} = \frac{Q}{X} \quad \text{whence } P_X(\eta) = X P_X(Q). \tag{38}$$
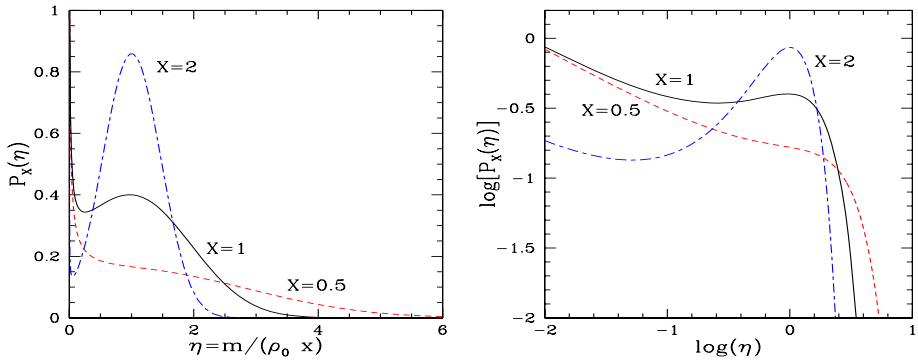
Fig. 5 (Color online) *Left panel:* The probability distribution $P_X(\eta)$ of the overdensity $\eta = m/(\rho_0 x) = Q/X$, for three Eulerian sizes, $X = 0.5, 1$ and 2, from (18), (38). All curves display an inverse square root singularity $\propto 1/\sqrt{\eta}$ at small densities $\eta \to 0^+$. In addition, there is a Dirac contribution, $P_X^0 \delta(\eta)$, with the weight P_X^0 displayed in Fig. 12, associated with empty cells. At large scales X we recover a distribution that is sharply peaked around the mean density, $\langle \eta \rangle = 1$ (i.e. $\langle \rho \rangle = \rho_0$). *Right panel:* Same as *left panel* but on a logarithmic scale

Explicit expressions are obtained by substituting (108) and (18). In particular, the singular part (108) gives the Dirac contribution $P_X^0 \delta(\eta)$ associated with empty cells. For the regular part, $\eta > 0$, the asymptotic behaviors at large and small scales are directly read from (19)–(23) as

$$X \gg 1: \quad P_X(\eta) \sim \frac{X}{\text{Ai}'(-\omega_1)^2} \, \eta^{-1/2} \, e^{-\omega_1 X - X^3/12} \quad \text{for } \eta \ll X^{-3}, \tag{39}$$

$$P_X(\eta) \sim \frac{\sqrt{\pi} X^{5/2}}{\text{Ai}'(-\omega_1)^2} \, |\eta - 1|^{3/2} \, e^{-\omega_1 X |\eta - 1| - X^3 |\eta - 1|^3/12}$$

$$\text{for } |\eta - 1| \gg X^{-1} \text{ and } \eta \gg X^{-3}, \tag{40}$$

and

$$X \ll 1: \quad P_X(\eta) \sim \frac{X^{3/2}}{\sqrt{\pi}} \, \eta^{-1/2} \qquad\qquad \text{for } \eta \ll X^{-1}, \tag{41}$$

$$P_X(\eta) \sim 2\sqrt{\pi} X^{9/2} \eta^{5/2} e^{-\omega_1 X \eta - X^3 \eta^3/12} \quad \text{for } X^{-1} \ll \eta \ll X^{-3/2}, \tag{42}$$

$$P_X(\eta) \sim 2\pi X^3 \eta^{3/2} e^{-\omega_1 X \eta - X^3 \eta^3/12} \quad\quad \text{for } \eta \gg X^{-3/2}. \tag{43}$$

Thus, at all scales we have an inverse square root tail at low densities, $\propto 1/\sqrt{\eta}$, that follows from the low-Q tail obtained in Sect. 4.1. Again, its weight shows the same cubic exponential decay at large scales as the weight P_X^0 of empty cells (109), whereas at small scales it describes the full low-density regime. On large scales, the density distribution is centered on the mean $\langle \eta \rangle = 1$, with cubic exponential tails on both sides, until it reaches the very low-density tail $\propto 1/\sqrt{\eta}$ at $\eta \ll 1/X^3$. On small scales the density distribution shows a monotonous decline, with again a cubic exponential tail at large densities, $\eta \gg 1/X$. We display the density distribution $P_X(\eta)$ in Fig. 5, for three Eulerian sizes as in Fig. 1, to show its evolution with scale. Again, the cubic exponential tails (40) and (43) can be obtained from a simple and general steepest-descent method [33]. However, the exponent $-1/2$ of

the power-law regime that appears at small scales in (41) is beyond the reach of such methods. It would be interesting to build general approaches that would be able to describe this highly nonlinear regime, for generic initial conditions and dimensions. Then, the result (41) would allow one to check the accuracy of such a method for a nontrivial case.

From the results of Sect. 4.2, we can see that on large scales the distribution of the overdensity is described by the asymptotic distribution

$$X \gg 1: \quad P_X(\eta) \sim X \, \mathcal{F}_\infty(X(\eta - 1)), \tag{44}$$

which is increasingly peaked around $\eta = 1$ at larger scales. Thus, we recover as expected the uniform density ρ_0 on large scales, with a distribution that falls off faster than a Gaussian, as $e^{-X^3|\eta-1|^3/12}$. Since $\eta = Q/X = 1 - V/X$, we obtain from (28)–(29) for the moments of the density in this large-X limit:

$$X \gg 1: \quad \langle (\eta - 1)^{2n+1} \rangle = 0,$$

$$\langle (\eta - 1)^{2n} \rangle = \frac{(-1)^n}{X^{2n}} \, \hat{\mathcal{F}}_\infty^{(2n)}(0), \quad \text{whence } \langle \eta \rangle = 1, \, \langle \eta^2 \rangle_c \simeq \frac{0.837}{X^2}. \tag{45}$$

In agreement with the conservation of matter we can check that $\langle \eta \rangle = 1$.

On small scales we obtain from Sect. 4.3

$$X \ll 1: \quad P_X(\eta) \sim X^2 \mathcal{F}_0(X\eta), \quad \text{and for } \nu > 0:$$

$$\langle \eta^\nu \rangle \sim X^{-\nu+1} \, \Gamma[\nu + 1] \int_{-i\infty}^{+i\infty} \frac{\mathrm{d}s}{2\pi \mathrm{i}} \, (-s)^{-\nu-1} \, \tilde{\mathcal{F}}_0(s). \tag{46}$$

As seen in Sect. 4.3, the scaling function $\mathcal{F}_0(Q)$ in (30) describes the probability distribution of the Lagrangian increment down to $Q = 0^+$, hence it also describes the probability distribution of the overdensity down to $\eta = 0^+$ in (46). Next, the moments of integer order are given by

$$X \ll 1, \, n \geq 1: \quad \langle \eta^n \rangle \sim X^{-n+1} \, (-1)^n \, \tilde{\mathcal{F}}_0^{(n)}(0) \quad \text{whence } \langle \eta \rangle = 1, \, \langle \eta^2 \rangle \simeq \frac{1.136}{X}, \tag{47}$$

which gives the cumulant hierarchy

$$X \ll 1, \, n \geq 1: \quad S_n(X) = \frac{\langle \eta^n \rangle_c}{\langle \eta^2 \rangle_c^{n-1}} \sim (-1)^n \, \frac{\tilde{\mathcal{F}}_0^{(n)}(0)}{\tilde{\mathcal{F}}_0''(0)^{n-1}}. \tag{48}$$

Thus, the ratios $S_n(X)$ have a finite limit for $X \to 0$ and the cumulant generating function $\varphi_X(y)$ can be written as

$$X \ll 1: \quad \varphi_X(y) = \sum_{n=1}^{\infty} (-1)^{n-1} S_n(X) \frac{y^n}{n!} \sim -\tilde{\mathcal{F}}_0''(0) \left[\tilde{\mathcal{F}}_0 \left(\frac{y}{\tilde{\mathcal{F}}_0''(0)} \right) - \tilde{\mathcal{F}}_0(0) \right]. \tag{49}$$

As explained in Sect. 4.3, the scalings (46)–(49) are due to the presence of shocks and are therefore quite general: they apply as soon as shocks have formed with a finite probability, for any initial conditions. We discuss these small-scale scalings in Sects. 7.2 and 7.3 below, for more general initial conditions and higher dimensions.

We can note that on large scales the ratios $S_n(X)$ go to zero for odd n and diverge for even n, as seen from (45). This is due to the fact that, even though we start with Gaussian
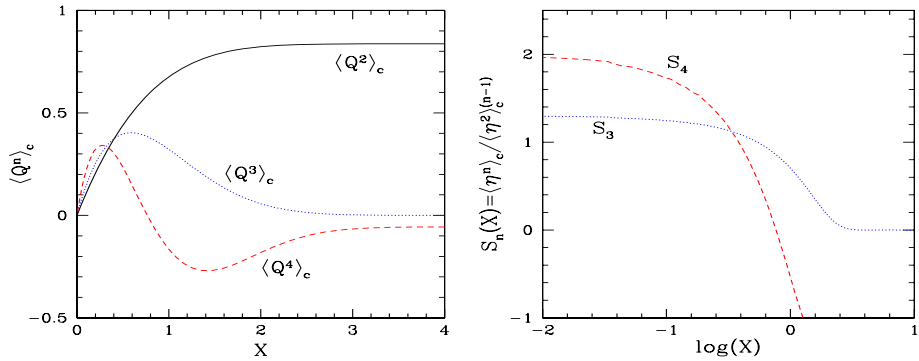
Fig. 6 (Color online) *Left panel:* The first few cumulants $\langle Q^n \rangle_c$ of the Lagrangian increment Q, as a function of the dimensionless scale $X = x/(2Dt^2)^{1/3}$. *Right panel:* The ratios S_n, defined by the first equality in (48), as a function of X on a semi-logarithmic scale

initial conditions at $t = 0$, the initial energy spectrum is so "blue" (which also leads to a singular white-noise initial velocity) that at any time $t > 0$ the system is strongly affected by nonlinear effects (associated with the building of isolated shocks amid empty regions). This regularizes the density distribution, $p_x(\eta)$, but the latter remains non-Gaussian in the large-scale limit $x \to \infty$, as seen in (44)–(45) or the explicit expression (40). Thus, we have $\langle \eta^{2n} \rangle_c \sim \langle \eta^2 \rangle_c^n$ and $S_{2n}(X) \sim \langle \eta^2 \rangle_c^{1-n} \sim X^{2(n-1)}$, for $n \geq 1$ and $X \to \infty$, whereas odd cumulants are exponentially small. By contrast, for initial conditions with a sufficiently "red" spectrum, such as the Brownian case, the density distribution becomes Gaussian on large scales (it remains governed by the initial field and linear theory) and the ratios $S_n(X)$ have a finite large-scale limit that can be computed through perturbative means, see [33, 34].

We show in Fig. 6 the first few cumulants $\langle Q^n \rangle_c$ and ratios S_n. As explained above and in Sect. 4.2, at large scales both $\langle Q^2 \rangle_c$ and $\langle Q^4 \rangle_c$ reach a nonzero value, as the large-scale distribution is non-Gaussian, whereas the odd cumulant $\langle Q^3 \rangle_c$ shows a cubic exponential decay, since the limiting scaling function $\mathcal{F}_\infty$ is even. At small scale all cumulants show a linear dependence on X, in agreement with (35). Then, the ratio S_3 also shows a cubic exponential decay on large scales whereas S_4 goes to $-\infty$; next on small scales both coefficients reach a nonzero asymptotic value.

5.2 Density Two-Point Correlation and Power Spectrum

We now consider the two-point correlation, $\xi(x, t)$, of the density field $\rho(x, t)$ itself:

$$\langle \rho(x_1, t)\rho(x_2, t) \rangle_c = \rho_0^2 \, \xi(x_2 - x_1, t), \quad \text{whence} \quad \langle \eta^2 \rangle_c = \int_0^x \frac{dx_1 \, dx_2}{x^2} \, \xi(x_2 - x_1). \quad (50)$$

In terms of the dimensionless variables (8), using $\eta = Q/X$, we obtain

$$\langle Q^2 \rangle - X^2 = \int_0^X dX_1 \, dX_2 \, \xi(X_2 - X_1), \quad \text{whence} \quad \xi(X) = \frac{1}{2} \frac{d^2}{dX^2} \langle Q^2 \rangle - 1. \quad (51)$$

Then, the small-distance behavior (35), that was associated with shocks, gives rise to a Dirac contribution

$$\xi^0(X) = \tilde{\mathcal{F}}_0''(0) \, \delta(X), \quad \text{whence} \quad \xi^0(x) = (2Dt^2)^{1/3} \tilde{\mathcal{F}}_0''(0) \, \delta(x) \simeq 1.136 \, (2Dt^2)^{1/3} \, \delta(x). \quad (52)$$

In terms of the density power spectrum, $\mathcal{P}(k, t)$, defined by

$$\rho(x, t) - \rho_0 = \int_{-\infty}^{\infty} \frac{dk}{2\pi} e^{ikx} \hat{\rho}(k, t), \quad \langle \hat{\rho}(k_1, t) \hat{\rho}(k_2, t) \rangle = \delta(k_1 + k_2) 2\pi \mathcal{P}(k_1, t), \quad (53)$$

this gives the asymptotic behavior at high k,

$$k \to \infty: \quad \mathcal{P}(k, t) \to \tilde{\mathcal{F}}_0''(0) (2Dt^2)^{1/3} \simeq 1.136 (2Dt^2)^{1/3}. \quad (54)$$

As expected, shocks, that form a series of Dirac peaks in the density field, give rise to a white-noise power spectrum in the limit of high wavenumbers. In addition, there are also nonzero correlations at finite distances, that can be obtained from the second cumulant of the Lagrangian increment Q through (51). Using the expression (18), making the change of variable $s_i \to s_i + s$ and integrating over Q and s, we obtain

$$\langle Q^2 \rangle = \frac{\partial^2}{\partial s^2}\bigg|_0 2\sqrt{\pi X} e^{-X^3/12} \int_{-i\infty}^{+i\infty} \frac{ds_1 \, ds_2}{(2\pi i)^2} \frac{e^{(s_1 + s_2)X/2 + (s_1 - s_2)^2/(4X)}}{\text{Ai}(s_1)\text{Ai}(s_2)\text{Ai}(s_1 + s)\text{Ai}(s_2 + s)}$$

$$\times \int_0^{\infty} dr \, e^{Xr} \text{Ai}(r + s_1 + s)\text{Ai}(r + s_2 + s). \quad (55)$$

Next, going back to $s_i \to s_i - s$, using the expression (111), which allows to remove the asymptotic X^2 behavior of $\langle Q^2 \rangle$, and differentiating twice with respect to X, the density two-point correlation reads as

$$X > 0: \quad \xi(X) = \sqrt{\pi} \int_{-i\infty}^{+i\infty} \frac{ds_1 \, ds_2}{(2\pi i)^2} \frac{1}{\text{Ai}(s_1)\text{Ai}(s_2)} \left\{ -A_{s_1, s_2}''(X) \int_X^{\infty} dy \, e^{-\Phi_{s_1, s_2}(y)} h_{s_1, s_2}(y) \right.$$

$$+ e^{-\Phi_{s_1, s_2}(X)} \left[2A_{s_1, s_2}'(X) h_{s_1, s_2}(X) + A_{s_1, s_2}(X)(h_{s_1, s_2}'(X) \right.$$

$$\left. \left. - \Phi_{s_1, s_2}'(X) h_{s_1, s_2}(X)) \right] \right\}, \quad (56)$$

where the functions $\Phi_{s_1, s_2}(X)$ and $h_{s_1, s_2}(X)$ are defined in (112)–(113) and we introduced the function $A_{s_1, s_2}(X)$ given by

$$A_{s_1, s_2}(X) = \frac{\partial^2}{\partial s^2}\bigg|_0 \frac{e^{-sX}}{\text{Ai}(s_1 - s)\text{Ai}(s_2 - s)}. \quad (57)$$

This yields the asymptotic behaviors

$$\xi(0) \simeq -0.56, \quad \text{and for } X \to \infty: \quad \xi(X) \sim \frac{-\sqrt{\pi}}{16\text{Ai}'(-\omega_1)^2} X^{11/2} e^{-\omega_1 X - X^3/12}. \quad (58)$$

Thus, as we can check in Fig. 7, the density correlation is negative for $x > 0$. This may be understood from the fact that, since the matter collapses within isolated zero-thickness objects (shocks), close to a shock there is a relative underdensity as matter has already fallen into that shock. In terms of particles of infinitesimal mass, the massive aggregate associated with the shock has swept matter from its neighborhood along its motion at previous times as particles stick together after collisions. Thus, starting with a white-noise initial velocity which shows no correlations over finite distance $x > 0$, some (anti-)correlations appear as soon as $t > 0$ over scales of order $x \sim (2Dt^2)^{1/3}$ (i.e. $X \sim 1$), but they remain very weak as
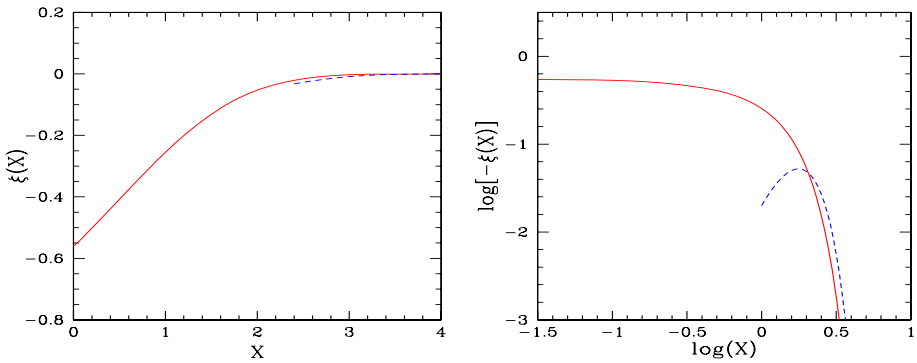
Fig. 7 (Color online) *Left panel:* The density two-point correlation, $\xi(x) = \langle \rho(x_1)\rho(x_1 + x) \rangle_c/\rho_0^2$, as a function of the dimensionless scale $X = x/(2Dt^2)^{1/3}$, from (56). It is negative over $x > 0$ but there is an additional Dirac contribution at the origin, given by (52). The *dashed line* is the large-X asymptotic behavior (58). *Right panel:* Same as *left panel* but on a logarithmic scale

they decay even faster than a Gaussian at larger scales. Again, the cubic exponential falloff (58) can be understood from simple arguments. Following the discussion above, correlations at scale x arise from the motion of shocks over distances of order x and the building of voids of size X. Then, as discussed below (109), this can be associated to an initial mean velocity $\bar{v}_0(x) \sim x/t$ over the interval x and to a probabilistic weight $\sim e^{-(x/t)^2/(D/x)} \sim e^{-x^3/(Dt^2)}$, which gives back the cubic exponential tail (58). In agreement with this discussion, we can check that the tail (58) is the same (apart from the power-law prefactor) as the one obtained in (109) for the probability of voids.

From (53) the density power spectrum can be written, in terms of dimensionless variables, as

$$\mathcal{P}(K) = 2 \int_0^\infty dX \, \cos(KX)\, \xi(X) + \tilde{\mathcal{F}}_0''(0) = 2 \int_0^\infty dX [\cos(KX) - 1]\xi(X), \quad (59)$$

where $K = \gamma k$ (and γ was defined in (8)). In the first equality we explicitly separated the Dirac contribution (52) from the integral over $X > 0$. The second equality follows by noticing that $\mathcal{P}(0) = 0$. Indeed, from (51) we have

$$\mathcal{P}(0) = \int_{-\infty}^\infty dX \, \xi(X) = \lim_{X \to \infty} \left[\frac{d}{dX} \langle Q^2 \rangle - 2X \right] = 0, \quad (60)$$

as the term in brackets decays as $e^{-X^3/12}$ at large X, as seen from Sect. 4.2 and Appendix C. We show in Fig. 8 our results for the power spectrum, using (56) and (59). We clearly see the quadratic behavior at low K, that can be obtained by expanding the cosine in (59), and the saturation at high wavenumbers to the white-noise spectrum (54) due to shocks. Since the correlation function decays faster than a Gaussian at large distances the power spectrum is actually regular at $k = 0$. The high-wavenumber behavior (54) is universal and appears as soon as shocks have formed, along with the scalings (35)–(36) for the Lagrangian and velocity increments observed on small scales. The quadratic low-k behavior applies from (59) to initial conditions such that the linear power on large scales decays faster than k^2 (by contrast, if the initial velocity field is given by a Brownian motion, which shows significant
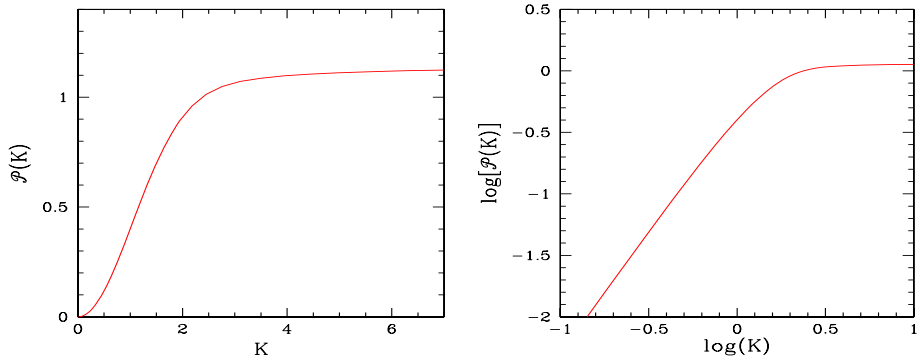
Fig. 8 (Color online) *Left panel:* The dimensionless density power spectrum $\mathcal{P}(K)$, as a function of the dimensionless wavenumber $K = (2Dt^2)^{1/3}k$, from (59). It goes to zero as K^2 at small K and it goes to a constant at large K. *Right panel:* Same as *left panel* but on a logarithmic scale

power on large scales, the density power spectrum is exactly a white-noise spectrum over all k, that is $\mathcal{P}(k)$ is constant down to $k = 0$).

Again, the results (56) and (59), shown in Figs. 7 and 8, may be useful to test general approximation schemes. In particular, in the cosmological context, the matter two-point correlation and power spectrum are among the main observables used to constrain cosmological scenarios (both the global cosmological history, through the linear growth factor of density fluctuations, and the primordial initial conditions, generated by an hypothetical inflationary stage, through the shape of the power spectrum). For gravitational systems of this sort, no good approximation scheme has been obtained yet that is able to estimate the density power spectrum in both linear and nonlinear regimes (i.e. from large down to small scales), so that one needs to use numerical simulations. The case studied in this article provides a rare hydrodynamical example, closely related to 1-D gravitational dynamics as recalled above, where a complete exact solution can be derived. In this respect, the present case of white-noise initial velocity is somewhat more interesting than the case of Brownian initial velocity, where the power spectrum is simply a constant over all scales, as it shows a transition between different low- and high-wavenumber regimes.

A key difference between Burgers dynamics and gravitational systems (and real turbulence) is that the high-k regime is quite simple and universal, since it is governed by shocks and shows a constant white-noise asymptote as in (54). By contrast, in 3-D gravitational (or Navier-Stokes) systems, small-scale structures may show a broader variety (extended halos, vortices, ...) [21, 36] and it is not known whether universal exponents exist and for which class of initial conditions they hold (in the cosmological context numerical simulations suggest that there is no such universality as the high-k slope seems to depend on the initial slope [26]).

6 Lagrangian Displacement Field

6.1 One-Point Distribution

We now consider the Burgers dynamics from a Lagrangian point of view, as opposed to the Eulerian point of view described in the previous sections. Thus, labeling the particles

by their initial position q at the initial time $t = 0$, we follow their trajectory $x(q, t)$. Since particles do not cross each other they remain well-ordered. Then, the probability, $p_q(\geq x)$, for the particle q to be located to the right of the position x, is equal to the probability, $p_x(\leq q)$, for the Lagrangian coordinate $q(x)$ associated with position x to be smaller than or equal to q. This yields

$$P_Q(X) = -\frac{\partial}{\partial X} P_X(\leq Q) = -\frac{\partial}{\partial X} \int_{-\infty}^{Q} dQ' \, P(Q' - X) = P(Q - X),$$

$$\text{whence } P_Q(X) = P_X(Q), \tag{61}$$

where we used from (102) the property that the Eulerian distribution $P_X(Q)$ only depends on the relative distance $Q - X$ as $P_X(Q) = P(Q - X)$ with $P(V)$ given by (102). Thus, the one-point Eulerian and Lagrangian distributions are identical. This applies to any initial conditions which are statistically homogeneous and isotropic, so that $P_X(Q)$ only depends on $|Q - X|$.

6.2 Two-Point Distribution and Relative Distance

We now investigate the two-point distribution of the Lagrangian displacement field. In a fashion similar to the one-point distribution, we can relate the Eulerian and Lagrangian distributions by

$$P_{Q_1, Q_2}(\geq X_1, \leq X_2) = P_{X_1, X_2}(\leq Q_1, \geq Q_2). \tag{62}$$

Then, for $Q_1 < Q_2$ the Dirac part (13) does not contribute and we obtain from (12), with $X_1 \leq X_2$,

$$P_{Q_1, Q_2}(\geq X_1, \leq X_2) = \int_{-\infty}^{Q_1} dQ'_1 \int_{Q_2}^{\infty} dQ'_2 \, \mathcal{J}(Q'_1 - X_1) \, \mathcal{J}(X_2 - Q'_2) \, \mathcal{H}_{X_1, X_2}(Q'_1, Q'_2). \tag{63}$$

Using (103) and (106), this yields

$$P_{Q_1, Q_2}(X_1, X_2) = -\frac{\partial^2}{\partial X_1 \partial X_2} 2\sqrt{\pi (X_2 - X_1)} \, e^{-(X_2 - X_1)^3/12}$$

$$\times \int_{-i\infty}^{+i\infty} \frac{ds_1 ds_2 ds'_1 ds'_2}{(2\pi i)^4} \frac{e^{(s_1 - s_2)Q_1 + (s'_2 - s'_1)Q_2}}{(s_1 - s_2)(s'_1 - s'_2)}$$

$$\times \frac{e^{-s_1 X_1 + s'_1 X_2 + (s_2 - s'_2)(X_1 + X_2)/2 + (s_2 - s'_2)^2/(4(X_2 - X_1))}}{\mathrm{Ai}(s_1)\mathrm{Ai}(s_2)\mathrm{Ai}(s'_1)\mathrm{Ai}(s'_2)}$$

$$\times \int_0^{\infty} dr \, e^{(X_2 - X_1)r} \, \mathrm{Ai}(r + s_2)\mathrm{Ai}(r + s'_2). \tag{64}$$

We can check that (64) is invariant through uniform spatial translations. Next, from $P_{Q_1, Q_2}(X_1, X_2)$ we can derive the distribution, $P_Q(X)$, of the relative Eulerian distance, $X = X_2 - X_1$. It only depends on the relative Lagrangian distance, $Q = Q_2 - Q_1$, through

$$P_Q(X) = \int_{-\infty}^{\infty} dX_1 \, P_{Q_1, Q_1 + Q}(X_1, X_1 + X). \tag{65}$$
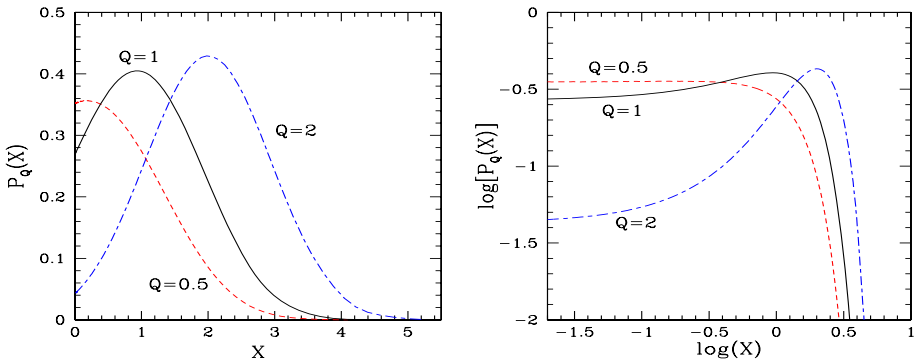
Fig. 9 (Color online) *Left panel:* The probability distribution $P_Q(X)$ of the Eulerian increment X, for three Lagrangian lengths, $Q = 0.5$, 1 and 2, from (68). The integral over $X > 0$ is smaller than unity as there is an additional Dirac contribution, $P_Q^{\text{shock}}\delta(X)$, associated with shocks, with the weight P_Q^{shock} displayed in Fig. 11. *Right panel:* Same as *left panel* but on a logarithmic scale

This gives

$$
X > 0: \quad P_Q(X) = \frac{\partial^2}{\partial X^2} 2\sqrt{\pi X}\, e^{-X^3/12} \int_{-i\infty}^{+i\infty} \frac{\mathrm{d}s\, \mathrm{d}s_1\, \mathrm{d}s_2}{(2\pi \mathrm{i})^3}
$$

$$
\times \frac{e^{s(Q-X)+(s_1+s_2)X/2+(s_1-s_2)^2/(4X)}}{s^2 \mathrm{Ai}(s_1)\mathrm{Ai}(s_2)\mathrm{Ai}(s_1-s)\mathrm{Ai}(s_2-s)}
$$

$$
\times \int_0^\infty \mathrm{d}r\, e^{Xr} \mathrm{Ai}(r+s_1)\mathrm{Ai}(r+s_2), \quad \text{with } \Re(s) < 0, \qquad (66)
$$

where the integration contour over s runs to the left of the pole at $s = 0$. Note that the expression (66) is similar to the result (18) obtained for the distribution of the Lagrangian increment Q over a fixed Eulerian interval X, except for the double derivative with respect to X and the factor $1/s^2$. This leads to the relationship between the distributions of the Eulerian and Lagrangian increments:

$$
\frac{\partial^2}{\partial Q^2} P_Q(X) = \frac{\partial^2}{\partial X^2} P_X(Q). \qquad (67)
$$

On the other hand, using the expression (111) and the comparison with (18), taking the derivatives with respect to X in (66) gives the relationship

$$
P_Q(X) = P_X(Q) + 2\sqrt{\pi} \int_{-i\infty}^{+i\infty} \frac{\mathrm{d}s\, \mathrm{d}s_1\, \mathrm{d}s_2}{(2\pi \mathrm{i})^3} \frac{e^{s(Q-X)}\, e^{-\Phi_{s_1,s_2}(X)}}{s^2 \mathrm{Ai}(s_1)\mathrm{Ai}(s_2)\mathrm{Ai}(s_1-s)\mathrm{Ai}(s_2-s)}
$$

$$
\times \left[-2s\, h_{s_1,s_2}(X) - \Phi'_{s_1,s_2}(X) h_{s_1,s_2}(X) + h'_{s_1,s_2}(X) \right]. \qquad (68)
$$

We show in Fig. 9 the distribution $P_Q(X)$ obtained for three Lagrangian intervals Q. In a fashion similar to the Eulerian distribution $P_X(Q)$ shown in Fig. 1, on large scales, $Q \gg 1$, the Lagrangian distribution $P_Q(X)$ is centered on Q, with cubic exponential tails on both sides as seen in (69) below, whereas on small scales, $Q \ll 1$, it shows a monotonous decline. However, contrary to the Eulerian distribution, the Lagrangian distribution $P_Q(X)$ does not
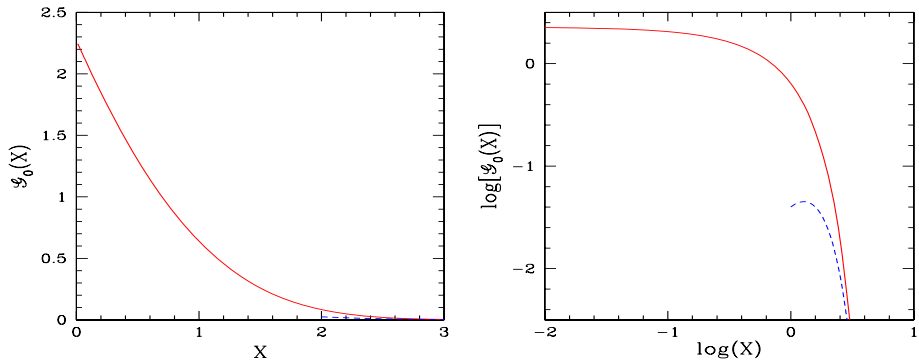
Fig. 10 (Color online) *Left panel:* The scaling function $\mathcal{G}_0(X)$ that describes the distribution of the Eulerian increment X in the limit $Q \ll 1$, from (70)–(71). The *dashed line* is the asymptotic behavior (72). *Right panel:* Same as *left panel* but on a logarithmic scale

show an inverse square-root tail at low X as $P_Q(0)$ is finite. As can be seen in Fig. 9, the distribution $P_Q(X)$ given by (66)–(68) over $X > 0$ is not normalized to unity as its weight decreases for smaller Q. Indeed, there is an additional Dirac contribution associated with shocks, of the form $P_Q^{\text{shock}} \delta(X)$, where the Eulerian increment X is zero (all particles in the initial range $[Q_1, Q_2]$, of length $Q = Q_2 - Q_1$, have merged into a single shock). Since the weight of this contribution grows at smaller Q, as can be checked in Fig. 11, the normalization of the regular contribution (66) decreases at smaller Q.

On large scales, $Q \gg 1$, from the expression (66) or the relation (67), we obtain

$$Q \gg 1: \quad P_Q(X) \sim \mathcal{F}_\infty(X - Q), \quad \text{whence } P_Q(X) \sim P_X(Q) \text{ for large } Q \text{ and } X, \quad (69)$$

where the function $\mathcal{F}_\infty$ was given in (25) and shown in Fig. 3. Thus, at large scales the distribution $P_Q(X)$ is peaked around $X = Q$, with fluctuations of order unity that become increasingly small as compared with Q for $Q \to \infty$. Moreover, it becomes identical to the Eulerian distribution in this limit.

On small scales, $Q \ll 1$, using the expression (111), we obtain a scaling similar to the one seen in (30) for the Eulerian distribution,

$$Q \ll 1: \quad P_Q(X) \sim Q \, \mathcal{G}_0(X), \quad \text{with } X > 0, \quad (70)$$

and

$$\mathcal{G}_0(X) = 2\sqrt{\pi} \int_{-i\infty}^{+i\infty} \frac{ds_1 \, ds_2}{(2\pi i)^2)} \frac{e^{-\Phi_{s_1,s_2}(X)}}{\mathrm{Ai}(s_1)^2 \mathrm{Ai}(s_2)^2} [\Phi'_{s_1,s_2}(X) h_{s_1,s_2}(X) - h'_{s_1,s_2}(X)]. \quad (71)$$

In particular, (71) gives the asymptotic behavior at large X:

$$X \gg 1: \quad \mathcal{G}_0(X) \sim \frac{\sqrt{\pi}}{8\mathrm{Ai}'(-\omega_1)^2} X^{7/2} e^{-\omega_1 X - X^3/12}. \quad (72)$$

We show the scaling function $\mathcal{G}_0(X)$ in Fig. 10. We can see that it is finite at $X = 0$ and is monotonically decreasing.

The scaling of (70) is related to the fact that the system is described by a finite number of shocks per unit length, with masses of order unity (in terms of the dimensionless variables

Q and X). Then, in the limit $Q \to 0$, the probability P_Q^{shock} that all particles in the interval $[Q_1, Q_2]$, of length $Q = Q_2 - Q_1$, belong to the same shock goes to unity, and there remains a probability of order Q that the particles Q_1 and Q_2 belong to different shocks, in which case their Eulerian distance is of order unity (i.e. $X \sim 1$). This gives rise to the scaling (70) for this contribution associated with $X > 0$. This discussion shows that the scaling (70) is less general than the scaling (30) obtained for the small-scale Eulerian distribution, since it relies on the fact that shocks are well separated by distances of order unity. For instance, in the case of Brownian initial velocity, the scaling (30) is still satisfied but the property (70) is no longer valid. Indeed, in this case shocks are dense in Eulerian space and the typical Eulerian distance X between particles initially separated by the Lagrangian distance Q scales as $X \sim \sqrt{Q}$, as can be seen in [34].

As discussed above, in addition to the contribution (66) associated with $X > 0$, there is a second contribution, of the form $P_Q^{\text{shock}} \delta(X)$, associated with the case where both particles Q_1 and Q_2 belong to the same shock, whence $X_2 = X_1$. Its weight can be derived by computing the weight $P_Q(X > 0)$ of the contribution (66). Integrating (66), which gives two boundary terms at $X = 0$ and $X = +\infty$, yields

$$P_Q(X > 0) = 1 - P_Q^{\text{shock}}, \quad \text{with } P_Q^{\text{shock}} = -2 \int_{-i\infty}^{+i\infty} \frac{ds\, ds'}{(2\pi i)^2} \frac{e^{sQ}}{s^2 \text{Ai}(s')^2} \frac{\partial}{\partial s'} \frac{\text{Ai}'(s' + s)}{\text{Ai}(s' + s)},$$
$$\Re(s) < 0, \tag{73}$$

where the integration contour over s runs to the left of the pole at $s = 0$. The comparison with (30)–(31) gives the relation

$$\frac{d^2}{dQ^2} P_Q^{\text{shock}} = \mathcal{F}_0(Q), \quad \text{whence } P_Q^{\text{shock}} = \int_Q^{\infty} dQ' \, (Q' - Q) \, \mathcal{F}_0(Q'). \tag{74}$$

In particular, using the results of Sect. 4.3, (74) gives at once the asymptotic behaviors

$$Q \to 0: \quad P_Q^{\text{shock}} \sim 1 - \tilde{\mathcal{F}}_0(0) \, Q \simeq 1 - 1.674 \, Q,$$
$$Q \to \infty: \quad P_Q^{\text{shock}} \sim 32\sqrt{\pi} \, Q^{-3/2} \, e^{-\omega_1 Q - Q^3/12}. \tag{75}$$

Thus, we recover the fact that the probability, P_Q^{shock}, for two particles of initial Lagrangian distance Q, to belong to the same shock, goes to unity for $Q \to 0$, with a linear deviation so that $P_Q(X > 0) \sim \tilde{\mathcal{F}}_0(0) Q$, in agreement with the scaling (70).

We display in Fig. 11 this probability P_Q^{shock}, which clearly shows its steep falloff at large Q. Again, the cubic exponential decay can be understood from the same arguments, as those used for the tails (11) or (109) of Eulerian distributions. Note that the formation of a single shock of strength $q = q_2 - q_1$ would be associated with a velocity difference $v_2 - v_1 = -q/t$, rather than with the mean velocity $\bar{v}_0$ over the length q as was the case for these Eulerian distributions. However, this difference does not give well-defined results for the initial white-noise velocity field. Again, this is due to the fact that the dynamics is governed by nonlocal processes, that is, one cannot obtain behaviors such as (75) from a local analysis (i.e. a local Taylor expansion) of the initial velocity field. This clearly follows from the fact that, at any time $t > 0$, matter has gathered in a series of discrete shocks, which has strongly modified the velocity field: the latter has been regularized by the balance between the (infinite) different sign velocities of neighboring particles over lengths of order $(2Dt^2)^{1/3}$ and become strongly non-Gaussian, as seen in Sects. B.1 and 4.2. However, to recover the tail (75), we can split the interval q into two equal parts, and note that at least
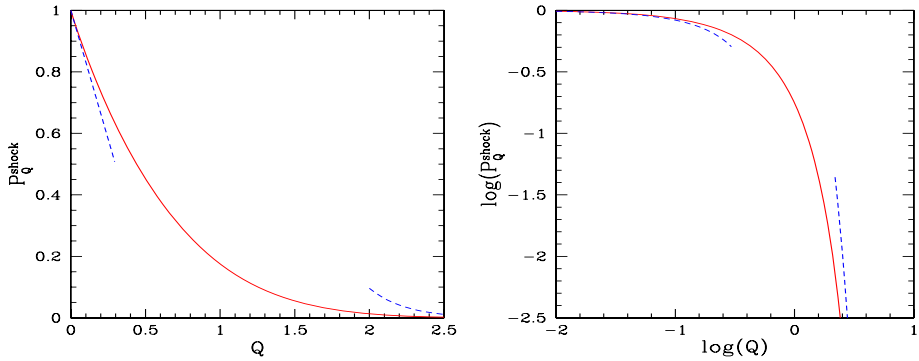
Fig. 11 (Color online) *Left panel:* The probability P_Q^{shock} that a Lagrangian interval of size Q has collapsed into a single shock, from (74). The *dashed line* is the asymptotic behavior (75). *Right panel:* Same as *left panel* but on a logarithmic scale

one of the two mean initial velocities $\bar{v}_1$ and $\bar{v}_2$ of both intervals must be of order q/t, which leads back to the cubic exponential tail (75).

6.3 Mass Function of Shocks

We briefly note here that the mass function of shocks, $n(m)$, can be derived from the shock probability p_q^{shock} studied in the previous section. Here we define $n(m)\,\mathrm{d}m$ as the mean number of shocks, per unit Eulerian or Lagrangian length (both functions are identical since on large scales $X = Q$ up to fluctuations of order unity, as seen in Sects. 4.2 and 6.2), with a mass in the range $[m, m + \mathrm{d}m]$. As in Sect. 5, since we consider a uniform initial density ρ_0, we have $m = \rho_0 q$ for the mass associated with a Lagrangian interval q. Then, the probability, p_q^{shock}, that two particles of initial Lagrangian distance q belong to the same shock, can be obtained by counting the number of shocks of mass $m \geq \rho_0 q$, each shock giving rise to a factor $(m/\rho_0 - q)$ as q_1 may be located within the distance $(m/\rho_0 - q)$ from its left boundary. In terms of dimensionless variables this reads as

$$P_Q^{\text{shock}} = \int_Q^\infty \mathrm{d}M\,(M - Q)N(M), \quad \text{with } n(m) = \frac{1}{\rho_0\gamma^2}N(M) \text{ and } M = \frac{m}{\rho_0\gamma}. \quad (76)$$

Then, using (74) we obtain at once

$$N(M) = \left.\frac{\mathrm{d}^2 P_Q^{\text{shock}}}{\mathrm{d}Q^2}\right|_{Q=M} = \mathcal{F}_0(M). \quad (77)$$

From the expression (32) we can check that we recover the result of [12], who directly derived the shock mass function from the geometrical construction (9) without considering the Lagrangian displacement field. This provides a useful check of the computations performed in Sect. 6.2 within a Lagrangian framework. The asymptotic properties of the shock mass function can also be read from (33), see also [2, 3, 12]. Moreover, the integral properties

$$\int_0^\infty \mathrm{d}M\,N(M) = \tilde{\mathcal{F}}_0(0) \simeq 1.674, \qquad \int_0^\infty \mathrm{d}M\,MN(M) = -\tilde{\mathcal{F}}_0'(0) = 1, \quad (78)$$

ensure that mass is conserved and that there is a finite mean number of shocks per unit length ($\simeq 1.674$ shocks in the mean, in units of X and Q). Many more properties of shocks, such as their n-point multiplicity functions as a function of their mass and velocity, can be found in [12].

7 Small-Scale Heuristic Approach for General Initial Conditions

The results obtained in the previous sections were derived from exact computations, based on (12) and (13). In this section, using a heuristic approach that assumes that small-scale properties are governed by shocks, or point-masses in higher dimensions, we discuss how small-scale scalings obtained for 1-D white-noise initial conditions would extend to generic initial conditions and higher dimensions.

7.1 General 1-D Case for the Distributions of Lagrangian and Velocity Increments on Small Scales

As explained in Sect. 4.3, the scalings $P_X(Q) \sim X \mathcal{F}_0(Q)$ and $\langle Q^\nu \rangle \propto X$ are due to the presence of shocks and as such they apply to a large class of initial conditions [14, 30]. Then, the distributions of the Lagrangian increment q and of the velocity increment v over the distance x are determined by the one-point distribution of shock strength [30], and they factorize as

$$x \to 0, \ q > 0, \ v < x: \quad p_x(q) \sim x\,n(q), \quad p_x(v) \sim xt\,n(x-v) \sim xt\,n(-v), \quad (79)$$

where $n(q)$ is the mass function of shocks, that is $n(q)\mathrm{d}q$ is the number of shocks of strength q per unit length. Here we used the dimensional variables x and q because the power of time that appears in the relevant scaling variables X and Q depends on the initial conditions. For instance, for a power-law initial energy spectrum, $E_0(k) \propto k^n$, with $-3 < n < 1$, we would have $X \propto x/t^{2/(3+n)}$ [18]. For initial energy spectra that are not a power law there may not exist scaling variables such as (8) (for instance, for a smooth spectrum one may expect a time-dependent effective exponent $n(t)$) but as soon as shocks are present one still has scalings of the form $\langle q^\nu \rangle \sim x$ at small distance for $\nu \geq 1$. Note that for $\nu = 1$ we always have the exact relation $\langle q \rangle = x$, because of the conservation of matter, but the linear scaling over x does not always extend to powers $0 < \nu < 1$, as for the white-noise case studied in the present paper, see (34). For instance, for Brownian initial velocity it only extends down to $\nu = 1/2$ [1, 34]. Indeed, as ν decreases the moment $\langle q^\nu \rangle$ becomes increasingly sensitive to low-density regions, characterized by low Lagrangian increment q, so that shocks are no longer dominant (for the white-noise case they remain dominant down to $\nu = 0^+$ because shocks are separated by voids where the Lagrangian increment q is exactly zero). It can be useful to introduce the moment generating function $\Psi_x(s)$, defined by

$$\Psi_x(s) = \sum_{n=1}^\infty \frac{(-s)^n}{n!} \langle q^n \rangle = \int_0^\infty \mathrm{d}q\,(e^{-sq} - 1)\,p_x(q), \quad (80)$$

whence

$$p_x(q) = \int_{-i\infty}^{+i\infty} \frac{\mathrm{d}s}{2\pi i}\, e^{sq}\,\Psi_x(s) \quad \text{for } q > 0, \quad (81)$$

where we assumed that all moments are finite and uniquely determine the function $\Psi_x(s)$ (note that adding a constant to $\Psi_x(s)$, so that $\Psi_x(0) \neq 0$, does not contribute to $p_x(q)$ for $q > 0$ as it only yields a Dirac $\delta(q)$). From the small-scale scaling (79) we obtain

$$x \to 0: \quad \Psi_x(s) \sim x\,\overline{\Psi}(s) \quad \text{and} \quad \langle q^n \rangle \sim x\,(-1)^n\,\overline{\Psi}^{(n)}(0),$$

$$\text{with } \overline{\Psi}(s) = \int_0^\infty dq\,(e^{-sq} - 1)\,n(q). \tag{82}$$

For the case of white-noise initial velocity studied in this article, using the dimensionless variables X and Q, we have $N(Q) = \mathcal{F}_0(Q)$ and $\overline{\Psi}(s) = \tilde{\mathcal{F}}_0(s) - \tilde{\mathcal{F}}_0(0)$, as shown by (30)–(31) and (77). For the case of Brownian initial velocity, using results from [34], we have

$$N(Q) = \frac{1}{\sqrt{\pi}}\,Q^{-3/2}\,e^{-Q}, \qquad \overline{\Psi}(s) = 2(1 - \sqrt{1+s}), \quad \text{for Brownian initial velocity,} \tag{83}$$

where we used the relevant scaling variables of the form $Q \propto q/t^2$ (here $E_0(k) \propto k^{-2}$). We can check in [34] that $N(Q)$, given in (83) as the shock mass function, also describes the probability distribution $P_X(Q)$ through $P_X(Q) \sim X N(Q)$ on small scales, as explained above in (79). Note that this remains valid even though shocks are no longer isolated but dense in Eulerian space. Indeed, if we select shocks above a small finite mass threshold m_*, the latter are again isolated so that the previous arguments apply, and smaller shocks only modify the low-q tail of the distribution. Indeed, the previous arguments hold for the limit $x \to 0$ at fixed q, or more precisely above a cutoff $q_-(x)$ that goes to zero faster than x, so that the scalings $\langle q^\nu \rangle \propto x$ for $\nu \geq 1$ do not depend on the behavior of the distribution $p_x(q)$ over this low-q domain. Thus, the functions $n(q)$ and $\overline{\Psi}(s)$ do not necessarily describe the actual distribution $p_x(q)$ down to $q = 0$ for a finite x. As seen above, for the case of white-noise initial velocity, the scaling function $\mathcal{F}_0(Q)$ of (30)–(31) actually applies down to $Q = 0^+$, as it only misses the Dirac contribution (108) (and the very high-Q tail (23) which is repelled to infinity). However, for the case of Brownian initial velocity for instance, the scaling functions (83) only apply to $Q \gg X^2$ and they miss a low-Q cutoff of the form $e^{-X^2/Q}$ [34].

7.2 General 1-D Case for the Distribution of Overdensities on Small Scales

As seen in Sect. 5.1, since the overdensity η is also given by the ratio $\eta = q/x$, its probability distribution is related to the distribution of the Lagrangian increment q through $p_x(\eta) = x p_x(q)$. Then, from (79)–(82) we have

$$x \to 0, \eta > 0: \quad p_x(\eta) \sim x^2\,n(x\eta) = x^2 \int_{-i\infty}^{+i\infty} \frac{ds}{2\pi i}\,e^{sx\eta}\,\overline{\Psi}(s). \tag{84}$$

If we define the cumulant ratios S_n and their generating function $\varphi_x(y)$ as in (48)–(49),

$$S_n(x) = \frac{\langle \eta^n \rangle_c}{\langle \eta^2 \rangle_c^{n-1}} \quad \text{and} \quad \varphi_x(y) = \sum_{n=1}^\infty (-1)^{n-1} S_n(x)\,\frac{y^n}{n!}, \tag{85}$$

using the property that in the small-scale limit, $x \to 0$, we have for $n \geq 1$ the asymptotic relationships $\langle \eta^n \rangle_c \sim \langle q^n \rangle/x^n$, we obtain

$$x \to 0: \quad \varphi_x(y) \sim \bar{\varphi}(y) \quad \text{with } \bar{\varphi}(y) = -\overline{\Psi}''(0)\,\overline{\Psi}\!\left(\frac{y}{\overline{\Psi}''(0)}\right), \tag{86}$$

and

$$x \to 0: \quad p_x(\eta) \sim - \int_{-i\infty}^{+i\infty} \frac{dy}{2\pi i \langle \eta^2 \rangle_c} e^{y\eta/\langle \eta^2 \rangle_c} \bar\varphi(y) \quad \text{with} \quad \langle \eta^2 \rangle_c = \frac{\overline{\Psi}''(0)}{x}. \quad (87)$$

We can check that this agrees with (49) for the white-noise initial velocity studied in this article. For the case of Brownian initial velocity [34], we have, in agreement with (83),

$$X \to 0: \quad P_X(\eta) \sim \sqrt{\frac{X}{\pi}} \, \eta^{-3/2} e^{-X\eta} \quad \text{and} \quad \bar\varphi(y) = \sqrt{1+2y} - 1,$$

$$\text{for Brownian initial velocity,} \quad (88)$$

where $X \propto x/t^2$ is again the scaling variable relevant to that initial condition. For the Brownian case it happens that the expression (88) for the density cumulant generating function is actually exact for all scales, but in the general case, as discussed below (83), it only applies to the small scale limit at fixed density contrast. More precisely, although $\mathcal{F}_0$ describes the overdensity probability distribution down to $\eta \to 0^+$ through (46) in the case of white-noise initial velocity, in the general case it only applies above a cutoff $\eta_-(x)$ that decreases with x (for instance for the Brownian initial velocity we have $\eta_-(x) \propto x$).

7.3 Multifractal Formalism in D Dimensions

These properties can be extended to higher dimensions D through a heuristic multifractal formalism [4, 13, 31], without going through the inverse Lagrangian map $\mathbf{x} \mapsto \mathbf{q}$. Thus, let us assume that the overdensity within a spherical cell of radius ℓ centered on $\mathbf{x}$ scales for $\ell \to 0$ as $\eta_\ell(\mathbf{x}) \sim \ell^\alpha$ for points $\mathbf{x} \in \mathcal{D}_\alpha \subset \mathbb{R}^D$, with $\dim\mathcal{D}_\alpha = F(\alpha)$. Then, we may write

$$\ell \to 0, \nu > 0: \quad \langle \eta_\ell^\nu \rangle = \int_0^\infty d\eta \, \eta^\nu \, p_\ell(\eta) \sim \int d\alpha \, \ell^{\nu\alpha + D - F(\alpha)} p_*(\alpha), \quad (89)$$

where $p_*(\alpha)$ gives the weight of the various multifractal exponents, and we used the fact that the probability for a sphere of radius ℓ to encounter an object of dimension F scales as ℓ^{D-F} for $\ell \to 0$. Using a steepest-descent argument, we obtain the small-scale exponents γ_ν,

$$\ell \to 0: \quad \langle \eta_\ell^\nu \rangle \sim \ell^{-\gamma_\nu} \quad \text{with} \quad \gamma_\nu = -\min_\alpha [\nu\alpha + D - F(\alpha)] = \max_\alpha [F(\alpha) - \nu\alpha - D]. \quad (90)$$

Thus, the exponents γ_ν and $F(\alpha)$ are related by a Legendre transform. The fractal scaling exponent α_ν that is associated to γ_ν through (90) is the abscissa of the first-contact point of the curve $F(\alpha)$ with the family of straight lines, $\nu\alpha + c$, moving downward from $c = +\infty$, in a fashion similar to the geometrical construction associated with (3). In particular, the exponents γ_ν only probe the concave hull of $F(\alpha)$ [13]. Since the matter density is positive the scaling exponents α_ν are restricted to $\alpha \geq -D$. This lower bound corresponds to Dirac density peaks (i.e. massive points), which have a zero dimension, $F(-D) = 0$. On the other hand, the constraint associated with the conservation of matter, $\langle \eta_\ell \rangle = 1$ whence $\gamma_1 = 0$, ensures that the curve $F(\alpha)$ is below the straight line $\alpha + D$, which runs through the point $\{-D, 0\}$, and has at least one contact point with this line. Then, we can see that, as soon as isolated Dirac density peaks have formed, with a finite probability per unit volume, the first-contact point between $F(\alpha)$ and the family of straight lines $\nu\alpha + c$ with $\nu \geq 1$ is the point $\{-D, 0\}$ (for $\nu = 1$ there can be other additional contact points), which gives $\gamma_\nu = (\nu - 1)D$ for $\nu \geq 1$. For instance, in three dimensions $D = 3$, we generically expect to first form

"Zeldovich pancakes" [37], that is sheets with a finite surface density, that intersect to form filaments (i.e. lines of finite line density), which join to form point-like masses (nodes). This corresponds to objects of fractal exponents and dimensions $\{-1, 2\}$, $\{-2, 1\}$, and $\{-3, 0\}$, along the line $\{\alpha, F = \alpha + D\}$, that all contribute to $\gamma_1 = 0$ while only point-like masses contribute to $\gamma_\nu = 3(\nu - 1)$ for $\nu > 1$. Then, we obtain

$$n \geq 1: \quad \langle \eta^n \rangle \sim \ell^{-(n-1)D} \quad \text{whence } \langle \eta^n \rangle_c \sim \ell^{-(n-1)D}, \, S_n(\ell) \sim \ell^0 \text{ and } \varphi_\ell(y) \sim \bar{\varphi}(y)$$

$$\text{for } \ell \to 0, \tag{91}$$

where the limiting generating function $\bar{\varphi}(y)$, reached in the small-scale limit, no longer depends on ℓ. Thus, for stochastic initial conditions, where we generically expect the formation of isolated Dirac density peaks in finite numbers per unit volume, we obtain the scaling (91) and the first expression in (87) for the density probability distribution, where in dimension D we have $\langle \eta^2 \rangle_c \sim \ell^{-D}$. As explained above, within this heuristic multifractal formalism the property (91) holds independently of the form of the fractal spectrum $F(\alpha)$ over $\alpha > -D$, as soon as there is a finite density of point-like masses which gives rise to the fractal exponent $\{\alpha = -D, F = 0\}$. The computation of the complete spectrum of fractal dimensions, that is necessary for the study of exponents $\nu < 1$ in (89), is a difficult task and in the general case there can be a continuous rather than discrete spectrum (as discussed below in a phenomenological fashion for the case of Brownian initial velocity, where shocks are dense).

Again, the scaling function $\bar{\varphi}(y)$ and the distribution it defines through (87) only apply above a density threshold $\eta_-(\ell)$ that may only show a very slow decrease with ℓ. Within the multifractal formalism (89) the behavior at small densities, below this threshold $\eta_-(\ell)$, depends on the properties of the curve $F(\alpha)$ to the right of the point $\{-D, 0\}$, see [4, 31]. For the one-dimensional case with white-noise initial velocity studied in this article, since shocks form isolated density peaks amid empty space, the curve $F(\alpha)$ is reduced to the single point $\{-1, 0\}$ so that the scalings $\langle \eta^\nu \rangle \sim X^{1-\nu}$ apply to all $\nu > 0$, in agreement with the second relation in (46) and the fact that the distribution $P_X(\eta) \sim X^2 \mathcal{F}_0(X\eta)$ in (46) applies downto $\eta = 0^+$, as seen in the previous sections.

For the one-dimensional case with Brownian initial velocity, we have the bifractality $\langle q^\nu \rangle \sim x$ for $\nu \geq 1/2$ and $\langle q^\nu \rangle \sim x^{2\nu}$ for $\nu \leq 1/2$ [1, 34]. This leads to $\langle \eta^\nu \rangle \sim x^{1-\nu}$ for $\nu \geq 1/2$ and $\langle \eta^\nu \rangle \sim x^\nu$ for $\nu \leq 1/2$. In terms of the multifractal formalism, this would be interpreted as a second point $\{1, 1\}$. This may be understood as follows. For these initial conditions, the shock mass function diverges at small masses as $n(m) \propto m^{-3/2}$ and shocks are uncorrelated and dense in Eulerian space [6, 28, 29, 34]. Then, choosing a small finite mass threshold m_*, the set of shocks of mass larger than m_* gives a population of isolated point-like masses that gives rise to the fractal exponent $\{-1, 0\}$. On the other hand, if we choose a random Eulerian interval of size ℓ, it contains in the mean $m^{-1/2}\ell$ shocks of mass in the range $[m, 2m]$. Taking $m \sim \ell^\beta$ we obtain that (i) for any $\beta > 2$ an interval of size ℓ contains of the order of $\ell^{1-\beta/2}$ shocks of mass in $[m, 2m]$, which leads to an overdensity larger than $\eta_\ell \sim \ell^{\beta/2}$, and (ii) for any $\beta < 2$ an interval of size ℓ contains with a probability of order $\ell^{1-\beta/2}$ at least one shock of mass in the range $[m, 2m]$, which leads to an overdensity larger than $\eta_\ell \sim \ell^{\beta-1}$. The first point (i) leads to the multifractal point $\{1, 1\}$, and the second point (ii) leads to the points $\{\beta - 1, \beta/2\}$ for $0 < \beta < 2$, that is to the segment joining the points $\{-1, 0\}$ and $\{1, 1\}$. Therefore, we obtain in this case the multifractal spectrum $F(\alpha) = \alpha/2 + 1/2$ with $-1 \leq \alpha \leq 1$, see also [1] for more rigorous discussions. More generally, in one dimension the scalings obtained for $\nu < 1$ and the low-density tail are related to the low-mass tail of the shock mass function.

We can note that the small-scale limit of finite ratios S_n and generating function $\varphi_x(y)$, as in (86), also corresponds to the "stable-clustering ansatz" introduced in the cosmological context as a phenomenological model for the highly nonlinear regime [27]. There, it was derived by assuming that on small physical scales, after nonlinear collapse and gravitational relaxation, overdensities decouple from the Hubble expansion and keep a constant physical size [10]. It can also be associated with a multifractal formalism, where the moments of the density with $\nu \geq 1$ would be governed by a single fractal exponent as in (91), which however would not be associated with point-like masses but with structures of exponent $\alpha \sim 1.3$ and dimension $F = 3 - \alpha \sim 1.2$ [4, 31]. However, contrary to the Burgers dynamics, this behavior may not be exactly reached on small scales for the gravitational dynamics, as the coefficients S_n still appear to show a weak dependence with scale [9]. On the other hand, the Burgers dynamics itself is also known as the "adhesion model" in this cosmological context [17, 35], where it provides a good description of the large-scale filamentary structure of the cosmic web [23]. It is not clear whether the reasonably good match of the "stable-clustering ansatz" could be understood from the exact scaling (91) achieved in the small-scale limit by the "adhesion model", since the nonlinear structures are different (point-like masses as opposed to extended halos) and no detailed comparisons have been performed yet in terms of the ratios S_n themselves.

8 Conclusion

We have obtained in this article some equal-time properties of the Burgers dynamics, in the inviscid limit for white-noise initial velocity. In agreement with previous works, the initially singular distributions are regularized as soon as $t > 0$, but little power is transferred to large scales. Thus, the distributions of the fluctuations of the Lagrangian increment, q, and of the velocity increment, v, around their means, have a finite limit in the large-scale limit $x \to 0$. We recover the characteristic cubic exponential tails associated with white-noise initial conditions. Voids lead to an additional Dirac-type contribution to these distributions, that also decays as a cubic exponential at large scales and is preceded by an inverse square root tail with a weight of the same order. On small scales, where the probability to be within a void goes to unity, the regular part factorizes as $X \mathcal{F}_0(Q)$, which corresponds to the probability to contain one shock of strength Q. In particular, the scaling function $\mathcal{F}_0(Q)$ is also the mass function of shocks. This leads to the standard linear scaling with x of the velocity structure functions at small scale, due to shocks.

Next, we have derived the distribution of the density within intervals of size x. It presents similar properties to those obtained for the Lagrangian increment, and exhibits the corresponding large-scale and small-scale scalings. In particular, at small scales this gives rise to the scaling hierarchy for the density cumulants known as the "stable-clustering ansatz" in cosmology. Here it is due to the presence of shocks. We also obtain the density two-point correlation and power spectrum, with the high-wavenumber constant asymptote associated with shocks.

Turning to the Lagrangian displacement field, associated with a description of the dynamics in terms of Lagrangian coordinates, we have obtained the distribution of the Eulerian increment x for a given mass $\rho_0 q$. On large scales the Lagrangian distribution $p_q(x)$ becomes identical, at leading order, to the Eulerian distribution $p_x(q)$. On small scales there is also a factorization of the form $Q \mathcal{G}_0(X)$, but this is less general than for the small-scale Eulerian distribution since it only applies to initial conditions such that shocks are isolated, that is initial energy spectra with $-1 < n < 1$, whereas the Eulerian factorization remains

valid for the whole range $-3 < n < 1$. Contrary to the Eulerian distribution, the Lagrangian distribution $p_q(x)$ does not show divergent tails as it remains finite for $x \to 0$, but there is again an additional Dirac contribution, which is now due to shocks.

Finally, within a heuristic approach we have discussed how these small-scale properties generalize to other initial conditions and give rise to a universal scaling for the distribution of the Lagrangian increment (and of the velocity increment) above a lower cutoff $q_-(x)$, that goes to zero faster than x in a fashion that depends on the initial conditions. A heuristic multifractal formalism allows to extend these results to higher dimensions. It generically leads to a universal scaling hierarchy for the density cumulants in the small-scale limit, that is governed by point-like masses. This also corresponds to the "stable-clustering ansatz" introduced in the cosmological context, where the Burgers dynamics is known as the "adhesion model" and is used to describe the large-scale cosmic web.

The results obtained in this article may prove useful to test approximation schemes devised to handle other initial conditions or closely related dynamics, such as Navier-Stokes turbulence or gravitational dynamics, where no exact results are available, as in [11, 32, 33]. In this respect, the case of white-noise initial velocity studied here would present a severe test for nonperturbative methods. Indeed, the initial energy spectrum is so "blue" that nonlinear effects are dominant up to the largest scales, $x \to \infty$, and perturbative expansions already encounter ultraviolet divergences at leading orders. This implies that alternative approaches must be able to take into account shocks, as for the steepest-descent methods presented in [33]. Another interesting feature of the case of white-noise initial velocity studied in this article is that it shows a density power spectrum that displays two different large-scale and small-scale regimes, as for the gravitational dynamics in the cosmological context, but can still be computed exactly.

Appendix A: Transition Kernel with Parabolic Absorbing Barrier

For the white-noise initial conditions (5), the process $q \mapsto \psi_0$ is Markovian and a key quantity is the conditional probability density $K_{x,c}(q_1, \psi_1; q_2, \psi_2)$ for the Markov process $\psi_0(q)$, starting from ψ_1 at q_1, to end at ψ_2 at $q_2 \geq q_1$, while staying above the parabolic barrier, $\psi_0(q) > \mathcal{P}_{x,c}(q)$, for $q_1 \leq q \leq q_2$. We briefly recall here its derivation, obtained in [12], using our notations. It obeys the diffusion equation

$$q_2 \geq q_1: \quad \frac{\partial}{\partial q_2} K_{x,c}(q_1, \psi_1; q_2, \psi_2) = \frac{D}{2} \frac{\partial^2}{\partial \psi_2^2} K_{x,c}(q_1, \psi_1; q_2, \psi_2) \quad (92)$$

over the domain $\psi \geq \mathcal{P}_{x,c}(q)$, with the initial condition at $q_2 = q_1$, $K_{x,c}(q_1, \psi_1; q_1, \psi_2) = \delta(\psi_2 - \psi_1)$, and the boundary conditions, $K_{x,c}(q_1, \psi_1; q_2, \psi_2) = 0$ for $\psi_1 = \mathcal{P}_{x,c}(q_1)$ or $\psi_2 = \mathcal{P}_{x,c}(q_2)$. The kernel associated with the propagation towards the left side, $q_2 \leq q_1$, is obtained from the parity symmetry

$$q_2 \leq q_1: \quad K_{x,c}(-q_1, \psi_1; -q_2, \psi_2) = K_{-x,c}(q_1, \psi_1; q_2, \psi_2). \quad (93)$$

In terms of the dimensionless coordinates (8) the kernel $K_{x,c}$ can be written as

$$K_{x,c}(q_1, \psi_1; q_2, \psi_2) \, d\psi_2 = e^{(Q_2-X)r_2 - (Q_1-X)r_1 - (Q_2-X)^3/3 + (Q_1-X)^3/3} \, G(\tau; r_1, r_2) \, dr_2, \quad (94)$$

where we defined

$$\tau = Q_2 - Q_1, \qquad r_i = 2\left[\Psi_i + \frac{(Q_i - X)^2}{2} - C\right], \quad (95)$$

and the propagator G obeys the Schrodinger-like equation

$$\frac{\partial G}{\partial \tau} = -r_2 \, G + \frac{\partial^2 G}{\partial r_2^2} \quad \text{over } \tau \geq 0, \ r \geq 0, \tag{96}$$

with the initial condition $G(0; r_1, r_2) = \delta(r_2 - r_1)$ and the boundary conditions $G(\tau; r_1, r_2) = 0$ for $r_1 = 0$ or $r_2 = 0$. This reduced propagator G can be solved as [12, 15]

$$G(\tau; r_1, r_2) = \sum_{k=1}^{\infty} e^{-\omega_k \tau} \frac{\text{Ai}(r_1 - \omega_k)\text{Ai}(r_2 - \omega_k)}{\text{Ai}'(-\omega_k)^2}, \tag{97}$$

where $-\omega_k$ are the zeros of the Airy function $\text{Ai}(x)$ (in particular, $\omega_1 \simeq 2.338$). Thus, $G(\tau; r_1, r_2)$ is symmetric over $\{r_1, r_2\}$, and it also obeys the backward equation (compare with (96))

$$\frac{\partial G}{\partial \tau} = -r_1 \, G + \frac{\partial^2 G}{\partial r_1^2} \quad \text{over } \tau \geq 0, \ r \geq 0. \tag{98}$$

Next, it is convenient to introduce the probability density, $E_{x,c}(q_1, \psi_1; q_2, \psi_2; q)\mathrm{d}q\mathrm{d}c\mathrm{d}\psi_2$, for the curve $\psi_0(q)$, starting from ψ_1 at q_1, to end at ψ_2 at $q_2 \geq q_1$, while staying above the parabolic barrier $\mathcal{P}_{x,c}$, and with a last excursion below $\mathcal{P}_{x,c+\mathrm{d}c}$ in the range $[q, q + \mathrm{d}q]$. From the definition of the kernel $K_{x,c}$, it reads as

$$E_{x,c}(q_1, \psi_1; q_2, \psi_2; q) = \frac{\partial}{\partial q} \lim_{\delta c \to 0} \frac{1}{\delta c} \int \mathrm{d}\psi [K_{x,c}(q_1, \psi_1; q, \psi)$$
$$- K_{x,c+\delta c}(q_1, \psi_1; q, \psi)] K_{x,c}(q, \psi; q_2, \psi_2). \tag{99}$$

Using a Taylor expansion and integrations by parts, this yields [12]

$$E_{x,c}(q_1, \psi_1; q_2, \psi_2; q) = \frac{D}{2} \frac{\partial K_{x,c}}{\partial \psi_2}(q_1, \psi_1; q, \psi) \frac{\partial K_{x,c}}{\partial \psi_1}(q, \psi; q_2, \psi_2)\bigg|_{\psi = \mathcal{P}_{x,c}(q)}, \tag{100}$$

which gives in terms of the reduced propagator G introduced in (94)

$$E_{x,c}(q_1, \psi_1; q_2, \psi_2; q) = \frac{8Dt^4}{\gamma^8} \, e^{(Q_2 - X)r_2 - (Q_1 - X)r_1 - (Q_2 - X)^3/3 + (Q_1 - X)^3/3}$$
$$\times \frac{\partial G}{\partial r_2}(Q - Q_1; r_1, 0) \frac{\partial G}{\partial r_1}(Q_2 - Q; 0, r_2). \tag{101}$$

As could be expected, the expression (101) shows that the probability density $E_{x,c}$ depends on the behavior of the propagator G close to the boundary $r = 0$ at one end. This corresponds to the contact point of abscissa q between the curve ψ_0 and the parabola $\mathcal{P}_{x,c}$ that is involved in the definition of $E_{x,c}$.

Appendix B: Eulerian Distributions

B.1 One-Point Distributions $p_x(q)$ and $p_x(v)$

Substituting (101) and (97) into (10), one obtains in terms of the dimensionless variables (8),

$$P_X(Q) = \mathcal{J}(X - Q)\,\mathcal{J}(Q - X) \quad \text{and} \quad P(V) = \mathcal{J}(V)\mathcal{J}(-V), \tag{102}$$

where we used the relation $X = Q + V$, with [12]

$$\mathcal{J}(u) = \lim_{\tau \to \infty} \int_0^\infty dr \, e^{-(\tau-u)^3/3+(\tau-u)r} \sum_{k=1}^\infty e^{-\omega_k \tau} \frac{\text{Ai}(r - \omega_k)}{\text{Ai}'(-\omega_k)} = \int_{-i\infty}^{+i\infty} \frac{ds}{2\pi i} \frac{e^{su}}{\text{Ai}(s)}. \quad (103)$$

From the asymptotic behaviors of the function $\mathcal{J}(u)$,

$$u \to +\infty: \quad \mathcal{J}(u) \sim \frac{e^{-\omega_1 u}}{\text{Ai}'(-\omega_1)}, \quad \text{and for } u \to -\infty: \quad \mathcal{J}(u) \sim -2u \, e^{u^3/3}, \quad (104)$$

one obtains the asymptotic behavior (11) of the distribution of the velocity V (and of the Lagrangian coordinate $Q = X - V$) [12].

B.2 Two-Point Distributions $p_{x_1,x_2}(q_1, q_2)$ and $p_{x_1,x_2}(v_1, v_2)$

We first consider the case (i) of Sect. 3.2, when the two first-contact parabolas $\mathcal{P}_{x_1,c_1}$ and $\mathcal{P}_{x_2,c_2}$ have two different contact points q_1 and q_2 with the curve $\psi_0(q)$ (and there is at least one shock in the interval $[x_1, x_2]$ since the map $x \mapsto q$ is constant outside of shocks [12, 28]). Then, noting q_* the abscissa of the intersection between both parabolas, in a fashion similar to (10) we can write this contribution to $p_{x_1,x_2}(q_1, q_2)$ as

$$p_{x_1,x_2}^{\neq}(q_1, q_2) = \lim_{q_\pm \to \pm\infty} \int dc_1 \, dc_2 \, d\psi_* \, d\psi_+ \, E_{x_1,c_1}(q_-, 0; q_*, \psi_*; q_1)$$
$$\times E_{x_2,c_2}(q_*, \psi_*; q_+, \psi_+; q_2). \quad (105)$$

Substituting the expression (101) of the kernel $E_{x,c}$ gives, in agreement with [12], the expression (12), where we introduced the function $\mathcal{H}$ defined by

$$\mathcal{H}_{X_1,X_2}(Q_1, Q_2) = 2(X_2 - X_1) \int_0^\infty dr_* \int_{Q_1}^{Q_2} dQ_* \, e^{(X_2-X_1)r_* - (Q_*-X_1)^3/3 + (Q_*-X_2)^3/3}$$
$$\times \frac{\partial G}{\partial r_1}(Q_* - Q_1; 0, r_*) \frac{\partial G}{\partial r_2}(Q_2 - Q_*; r_*, 0). \quad (106)$$

We can check that the function $\mathcal{H}_{X_1,X_2}(Q_1, Q_2)$, whence the distribution $P_{X_1,X_2}^{\neq}(Q_1, Q_2)$, are invariant with respect to uniform translations of X_i and Q_i, in agreement with the statistical homogeneity of the system.

We now consider the second case (ii) of Sect. 3.2, when the two parabolas intersect at the common point $q_1 = q_2$, and we can write this contribution to $p_{x_1,x_2}(q_1, q_2)$ as

$$p_{x_1,x_2}^{=}(q_1, q_2) = \delta(q_2 - q_1) \lim_{q_\pm \to \pm\infty} \lim_{q_* \to q_1^+} \int dc_1 \, d\psi_* \, d\psi_+ \, E_{x_1,c_1}(q_-, 0; q_*, \psi_*; q_1)$$
$$\times K_{x_2,c_2}(q_*, \psi_*; q_+, \psi_+). \quad (107)$$

This gives in terms of dimensionless variables [12] the expression (13).

B.3 Probability P_X^0 of Empty Intervals of Size X

Using (103), we can write the second term in (17) as [12]

$$P_X^{=}(Q) = \delta(Q) \, P_X^0 \quad \text{with } P_X^0 = \sqrt{\frac{\pi}{X}} \, e^{-X^3/12} \int_{-i\infty}^{+i\infty} \frac{ds_1 \, ds_2}{(2\pi i)^2} \frac{e^{(s_1+s_2)X/2+(s_1-s_2)^2/(4X)}}{\text{Ai}(s_1) \, \text{Ai}(s_2)}. \quad (108)$$
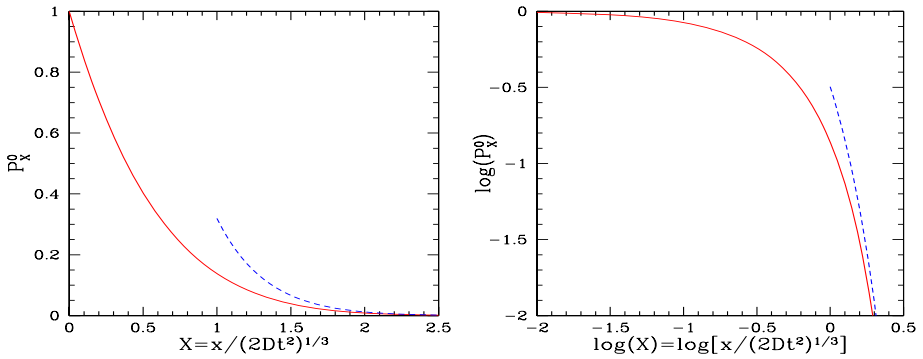
Fig. 12 (Color online) *Left panel:* The probability P_X^0 that an Eulerian interval of size X is empty, that is, that the Lagrangian increment Q over this interval is zero, from (108). The *dashed line* is the asymptotic behavior (109). *Right panel:* Same as *left panel* but on a logarithmic scale

This yields for the probability P_X^0 to have a vanishing Lagrangian increment the asymptotic behaviors

$$X \to 0: \quad P_X^0 \to 1, \quad \text{and for } X \to \infty: \quad P_X^0 \sim \frac{\sqrt{\pi}}{\text{Ai}'(-\omega_1)^2} X^{-1/2} e^{-\omega_1 X - X^3/12}. \quad (109)$$

Since Eulerian intervals with $Q = 0$ have a zero matter content, P_X^0 is also the probability for an interval of size X to be empty, in agreement with the result obtained in [12] for this void probability. We compare this probability P_X^0 with its asymptotic behavior (109) in Fig. 12, see also [12]. The cubic exponential tail (109) may be understood using the same arguments as those used for the tail of the velocity distribution (11) discussed above. Thus, for the Eulerian interval of size x to be empty, its initial matter content must have traveled by a distance of order x, which requires a mean velocity over this interval of order $v \sim x/t$. Again, since the initial Gaussian velocity over scale x is $\bar{v}_0(x) = (\psi_2 - \psi_1)/x$, with a variance $\sigma_{\bar{v}_0}^2(x) = D/x$, this yields the probability $\sim e^{-(x/t)^2/\sigma_{\bar{v}_0}^2(x)} \sim e^{-x^3/(Dt^2)}$, which gives back the cubic exponential tail (109).

Appendix C: Laplace Transform of the Product of Two Airy Functions

We recall here the results obtained by [12] for the integral over two Airy functions that appears in (18). Thus, if we define $f(r)$ and $g(x)$ by

$$f(r) = \text{Ai}(r + s_1)\text{Ai}(r + s_2), \qquad g(x) = \int_0^\infty dr\, e^{xr} f(r), \quad (110)$$

the Laplace transform $g(x)$ can be integrated as

$$g(x) = \frac{1}{2\sqrt{\pi}} e^{\Phi_{s_1,s_2}(x)} - e^{\Phi_{s_1,s_2}(x)} \int_x^\infty dy\, e^{-\Phi_{s_1,s_2}(y)} h_{s_1,s_2}(y), \quad (111)$$

with

$$\Phi_{s_1,s_2}(x) = \frac{x^3}{12} - \frac{s_1 + s_2}{2} x - \frac{1}{2} \ln x - \frac{(s_1 - s_2)^2}{4x}, \quad (112)$$

and

$$h_{s_1,s_2}(x) = \frac{f(0)}{4}x - \frac{f'(0)}{4} + \frac{f''(0) - 2(s_1 + s_2)f(0)}{4x}$$
$$- \frac{f^{(3)}(0) - 2(s_1 + s_2)f'(0) - 2f(0)}{4x^2}. \tag{113}$$

The first term in the right hand side of (111) gives the large-x behavior of $g(x)$, up to terms of relative order $e^{-x^3/12}$.

References

1. Aurell, E., Frisch, U., Noullez, A., Blank, M.: Bifractality of the devil's staircase appearing in the Burgers equation with Brownian initial velocity. J. Stat. Phys. **88**, 1151–1164 (1997)
2. Avellaneda, M.: Statistical properties of shocks in Burgers turbulence II: tail probabilities for velocities, shock-strengths and rarefaction intervals. Commun. Math. Phys. **169**, 45–59 (1995)
3. Avellaneda, M., Weinan, E.: Statistical properties of shocks in Burgers turbulence. Commun. Math. Phys. **172**, 13–38 (1995)
4. Balian, R., Schaeffer, R.: Scale-invariant matter distribution in the universe. II—Bifractal behaviour. Astron. Astrophys. **226**, 373–414 (1989)
5. Bec, J., Khanin, K.: Burgers turbulence. Phys. Rep. **447**, 1–66 (2007)
6. Bertoin, J.: The inviscid Burgers equation with Brownian initial velocity. Commun. Math. Phys. **193**, 397–406 (1998)
7. Burgers, J.M.: The Nonlinear Diffusion Equation. Reidel, Dordrecht (1974)
8. Cole, J.D.: On a quasi-linear parabolic equation occurring in aerodynamics. Quart. Appl. Math. **9**, 225–236 (1951)
9. Colombi, S., Bouchet, F.R., Hernquist, L.: Self-similarity and scaling behavior of scale-free gravitational clustering. Astrophys. J. **465**, 14 (1996)
10. Davis, M., Peebles, P.J.E.: On the integration of the BBGKY equations for the development of strongly nonlinear clustering in an expanding universe. Astrophys. J. Suppl. Ser. **34**, 425–450 (1977)
11. Fournier, J.-D., Frisch, U.: L'equation de Burgers deterministe et statistique. J. Mech. Theor. Appl. **2**, 699–750 (1983)
12. Frachebourg, L., Martin, Ph.A.: Exact statistical properties of the Burgers equation. J. Fluid Mech. **417**, 323–349 (2000)
13. Frisch, U.: Turbulence. Cambridge University Press, Cambridge (1995)
14. Frisch, U., Bec, J.: Burgulence. In: Lesieur, M., Yaglom, A., David, F. (eds.) Les Houches 2000: New Trends in Turbulence. Springer, Berlin (2001)
15. Groeneboom, P.: Brownian motion with a parabolic drift and airy functions. Probab. Theory Related Fields **81**, 79–109 (1989)
16. Gurbatov, S.N., Malakhov, A., Saichev, A.: Nonlinear Random Waves and Turbulence in Nondispersive Media: Waves, Rays and Particles. Manchester University Press, Manchester (1991)
17. Gurbatov, S.N., Saichev, A.I., Shandarin, S.F.: The large-scale structure of the universe in the frame of the model equation of non-linear diffusion. Mont. Not. R. Astron. Soc. **236**, 385–402 (1989)
18. Gurbatov, S.N., Simdyankin, S.I., Aurell, E., Frisch, U., Toth, G.: On the decay of Burgers turbulence. J. Fluid Mech. **344**, 339–374 (1997)
19. Hopf, E.: The partial differential equation $u_t + uu_x = u_{xx}$. Commun. Pure Appl. Math. **3**, 201–230 (1950)
20. Kida, S.: Asymptotic properties of Burgers turbulence. J. Fluid Mech. **93**, 337–377 (1979)
21. Kraichnan, R.H.: Lagrangian-history statistical theory for Burgers' equation. Phys. Fluids **11**, 265–277 (1968)
22. Le Doussal, P.: Exact results and open questions in first principle functional RG. arXiv:0809.1192 (2008)
23. Melott, A.L., Shandarin, S.F., Weinberg, D.H.: A test of the adhesion approximation for gravitational clustering. Astrophys. J. **428**, 28–34 (1994)
24. Molchan, G.M.: Burgers equation with self-similar Gaussian initial data: tail probabilities. J. Stat. Phys. **88**, 1139–1150 (1997)
25. Noullez, A., Gurbatov, S.N., Aurell, E., Simdyankin, S.I.: Global picture of self-similar and non-self-similar decay in Burgers turbulence. Phys. Rev. E **71**, 056305 (2005)

26. Peacock, J.A., Dodds, S.J.: Non-linear evolution of cosmological power spectra. Mon. Not. R. Astron. Soc. **280**, L19–L26 (1996)
27. Peebles, P.J.E.: The Large Scale Structure of the Universe. Princeton University Press, Princeton (1980)
28. She, Z.-S., Aurell, E., Frisch, U.: The inviscid Burgers equation with initial data of Brownian type. Commun. Math. Phys. **148**, 623–641 (1992)
29. Sinai, Ya.G.: Statistics of shocks in solutions of inviscid Burgers equation. Commun. Math. Phys. **148**, 601–621 (1992)
30. Tribe, R., Zaboronski, O.: On the large time asymptotics of decaying Burgers turbulence. Commun. Math. Phys. **212**, 415–436 (2000)
31. Valageas, P.: Non-linear gravitational clustering: smooth halos, substructures and scaling exponents. Astron. Astrophys. **347**, 757–768 (1999)
32. Valageas, P.: Using the Zeldovich dynamics to test expansion schemes. Astron. Astrophys. **476**, 31–58 (2007)
33. Valageas, P.: Quasi-linear regime and rare-event tails of decaying Burgers turbulence. Phys. Rev. E **80**, 016305 (2009)
34. Valageas, P.: Statistical properties of the Burgers equation with Brownian initial velocity. J. Stat. Phys. **134**, 589 (2009)
35. Vergassola, M., Dubrulle, B., Frisch, U., Noullez, A.: Burgers' equation, devil's staircases and the mass distribution for large-scale structures. Astron. Astrophys. **289**, 325–356 (1994)
36. Vogelsberger, M., White, S.D.M., Helmi, A., Springel, V.: The fine-grained phase-space structure of cold dark matter haloes. Mon. Not. R. Astron. Soc. **385**, 236–254 (2008)
37. Zeldovich, Y.B.: Gravitational instability: an approximate theory for large density perturbations. Astron. Astrophys. **5**, 84–89 (1970)